© 2015. Published by The Company of Biologists Ltd | Development (2015) 142, 1125-1136 doi:10.1242/dev.113829

RESEARCH ARTICLE

A *Grhl2*-dependent gene network controls trophoblast branching morphogenesis

Katharina Walentin[1,2], Christian Hinze[1,2], Max Werth[1,2,3], Nadine Haase[2], Saaket Varma[4], Robert Morell[5], Annekatrin Aue[1,2], Elisabeth Pötschke[1], David Warburton[4], Andong Qiu[3], Jonathan Barasch[3], Bettina Purfürst[1], Christoph Dieterich[6], Elena Popova[1], Michael Bader[1], Ralf Dechend[2], Anne Cathrine Staff[7], Zeliha Yesim Yurtdas[1,8,9], Ergin Kilic[10] and Kai M. Schmidt-Ott[1,2,11,*]

ABSTRACT

Healthy placental development is essential for reproductive success; failure of the feto-maternal interface results in pre-eclampsia and intrauterine growth retardation. We found that grainyhead-like 2 (GRHL2), a CP2-type transcription factor, is highly expressed in chorionic trophoblast cells, including basal chorionic trophoblast (BCT) cells located at the chorioallantoic interface in murine placentas. Placentas from *Grhl2*-deficient mouse embryos displayed defects in BCT cell polarity and basement membrane integrity at the chorioallantoic interface, as well as a severe disruption of labyrinth branching morphogenesis. Selective *Grhl2* inactivation only in epiblast-derived cells rescued all placental defects but phenocopied intraembryonic defects observed in global *Grhl2* deficiency, implying the importance of *Grhl2* activity in trophectoderm-derived cells. ChIP-seq identified 5282 GRHL2 binding sites in placental tissue. By integrating these data with placental gene expression profiles, we identified direct and indirect *Grhl2* targets and found a marked enrichment of GRHL2 binding adjacent to genes downregulated in $Grhl2^{-/-}$ placentas, which encoded known regulators of placental development and epithelial morphogenesis. These genes included that encoding the serine protease inhibitor Kunitz type 1 (*Spint1*), which regulates BCT cell integrity and labyrinth formation. In human placenta, we found that human orthologs of murine GRHL2 and its targets displayed co-regulation and were expressed in trophoblast cells in a similar domain as in mouse placenta. Our data indicate that a conserved *Grhl2*-coordinated gene network controls trophoblast branching morphogenesis, thereby facilitating development of the site of feto-maternal exchange. This might have implications for syndromes related to placental dysfunction.

[1]Max Delbrück Center for Molecular Medicine, Robert-Rössle-Str. 10, Berlin 13125, Germany. [2]Experimental and Clinical Research Center, a collaboration between the Max Delbrück Center and the Medical Faculty of the Charité, Robert-Rössle-Str. 10, Berlin 13125, Germany. [3]Department of Medicine, Columbia University College of Physicians and Surgeons, 630 West 168th Street, New York, NY 10032, USA. [4]Department of Developmental Biology and Regenerative Medicine Program, Saban Research Institute, Children's Hospital Los Angeles, 4650 Sunset Blvd., Los Angeles, CA 90027, USA. [5]Laboratory of Molecular Genetics, National Institute on Deafness and Other Communication Disorders (NIDCD)/National Institutes of Health (NIH), 5 Research Court, Rockville, MD 20850, USA. [6]Bioinformatics, Max Planck Institute for Biology of Ageing, Robert-Koch-Str. 21, Cologne 50931, Germany. [7]Department of Gynecology and Obstetrics, Institute of Clinical Medicine, Oslo University Hospital and University of Oslo, Kirkeveien 166, Oslo 0450, Norway. [8]Department of Urology, Charité-Universitätsmedizin Berlin, Charitéplatz 1, Berlin 10117, Germany. [9]Berlin Institute of Urologic Research, Berlin 10117, Germany. [10]Department of Pathology, Charité-Universitätsmedizin Berlin, Charitéplatz 1, Berlin 10117, Germany. [11]Department of Nephrology, Charité-Universitätsmedizin Berlin, Charitéplatz 1, Berlin 10117, Germany.

*Author for correspondence (kai.schmidt-ott@mdc-berlin.de)

Received 5 June 2014; Accepted 20 January 2015

KEY WORDS: Placenta defects, Epithelial differentiation, Epithelial morphogenesis, *Spint1*, Basement membrane defects

INTRODUCTION

The placenta facilitates the exchange of metabolites between mother and fetus. Pregnancy-associated diseases, such as pre-eclampsia and fetal intrauterine growth restriction (IUGR), affect up to 10% of pregnancies. The mouse placenta is a widely used model system (Adamson et al., 2002; Georgiades et al., 2002). Fetal trophectoderm-derived cells invade the maternal endometrium and form the site of feto-maternal exchange, which is referred to as the *villous tree* in humans and the *labyrinth* in mice. Both structures are formed by branching trophoblast cells accompanied by fetal blood vessels originating from the allantoic mesoderm (Cross et al., 2003b). This development facilitates a close apposition of fetal blood vessels to maternal blood sinuses and results in establishment of the feto-maternal barrier, which includes fetal endothelial cells and thin layers of trophoblast-derived syncytiotrophoblast (STB) cells. Pregnancy-associated diseases in humans commonly feature structural abnormalities of the villous tree and the feto-maternal barrier (Egbor et al., 2006).

In mice, labyrinth formation begins after chorioallantoic attachment at embryonic day (E) 8.5 through folding of the initially flat chorion and the formation of evenly distributed simple branches on the chorionic surface (Cross et al., 2003a). BCT cells initially form an epithelial-like cell layer with its basolateral surface facing the embryo. They form a basement membrane directly adjacent to the allantoic mesoderm. The BCT cell layer contains clusters of cells expressing the transcription factor GCM1, which define presumptive branch points. *Gcm1* expression is required for branching initiation and labyrinth formation, indicating that BCT cells act as central coordinators of these processes (Anson-Cartwright et al., 2000). Similar to BCT cells in mice, villous cytotrophoblasts in human placentas form a basement membrane adjacent to the extraembryonic mesoderm containing fetal blood vessels. Molecular cell type markers in mice suggest that BCT-derived cells differentiate and contribute to STB layer II (Simmons et al., 2008). Similarly, villous cytotrophoblasts are thought to differentiate into STB cells in humans. Hence, the villous cytotrophoblast layer in humans and the BCT layer in mice share functional and structural characteristics and appear to be crucial for morphogenesis and differentiation during placenta development. Homologies between human villous cytotrophoblasts and mouse BCT cells are also supported by molecular analyses. For instance, the serine protease inhibitor Kunitz type 1 (*Spint1*), an essential regulator of mouse placentation, displays high cell type-specific expression in the villous cytotrophoblasts of human placenta and in

Development (2015) 142, 1125-1136 doi:10.1242/dev.113829

BCT cells of mice (Hallikas et al., 2006; Szabo et al., 2007). Comparative genomics has shown that orthologs of over 80% of the genes known to be required for proper placental development in mice are also expressed in human placenta (Cox et al., 2009). The precise molecular programs driving branching morphogenesis, invasion and trophoblast differentiation remain incompletely understood.

Grainyhead-like transcription factors regulate the development of epithelial cell types in several species. They are implicated in epithelial morphogenesis, barrier formation and wound healing processes (Bray and Kafatos, 1991; Mace et al., 2005; Tao et al., 2005; Narasimha et al., 2008; Yu et al., 2009; Han et al., 2011; Gao et al., 2013). *Grhl2* is one of three mouse homologs of *Drosophila* Grainyhead (Wilanowski et al., 2002) and is expressed in diverse embryonic epithelial tissues during development (Wilanowski et al., 2002; Auden et al., 2006). *Grhl2* and its paralog *Grhl3* play essential roles in neural tube closure in mice (Rifat et al., 2010; Werth et al., 2010; Brouns et al., 2011; Pyrgaki et al., 2011). All three members regulate the expression of epithelial junctional genes (Yu et al., 2006; Wilanowski et al., 2008; Werth et al., 2010; Pyrgaki et al., 2011; Senga et al., 2012; Varma et al., 2012). We now report that *Grhl2* controls a target gene set in placental trophoblasts and is thereby crucial to placental morphogenesis.

RESULTS

Grhl2 ablation in mice perturbs placental labyrinth formation

We previously reported the generation of two mouse *Grhl2* null alleles: $Grhl2^{lacZ1}$ and $Grhl2^{lacZ4}$ (Werth et al., 2010). Whereas heterozygous $Grhl2^{+/lacZ1}$ and $Grhl2^{+/lacZ4}$ mice appeared normal, no live homozygous $Grhl2^{lacZ1/lacZ1}$ and $Grhl2^{lacZ4/lacZ4}$ mutants (collectively referred to as $Grhl2^{-/-}$) were recovered postnatally from heterozygous intercrosses (supplementary material Table S1). Until E11.5, the genotype distribution showed Mendelian ratios between $Grhl2^{+/+}$, $Grhl2^{+/-}$ and $Grhl2^{-/-}$. Analysis of embryos from timed heterozygous matings revealed that neural tube defects became apparent at E9.5 and IUGR at E10.5 in $Grhl2^{-/-}$ mutants. By E11.5, $Grhl2^{-/-}$ embryos were still present but had no visible heartbeat and displayed evidence of advanced tissue decay. We found no $Grhl2^{-/-}$ mutants after E11.5, indicating that *Grhl2* is crucial for embryonic development and survival past this stage.

To test the possibility that placenta defects contribute to this phenotype, we first analyzed GRHL2 expression by immunohistochemistry, which revealed robust levels in trophoblast cells from E7.5 to E16.5 (Fig. 1). We found high expression in the chorion at E7.5 and E8.0 (Fig. 1A-D). At E9.0, GRHL2 expression in the chorion became restricted to BCT cells (Fig. 1E,F). Moreover, GRHL2 was expressed in primary and secondary trophoblast giant cells (TGCs) (Fig. 1A-G,I) and in sinusoidal TGCs (S-TGCs) (Fig. 1H-J, arrows) of the chorion-derived labyrinth. By contrast, GRHL2 expression was low in the ectoplacental cone (Fig. 1A-D), but became more prominent as this structure developed into the spongiotrophoblast (Fig. 1G,I,J). We found no GRHL2 expression in the extraembryonic and allantoic mesoderm or in the maternal decidua (for an overview of the GRHL2 expression domain see Fig. 1K). No GRHL2 staining was present in $Grhl2^{-/-}$ placentas (supplementary material Fig. S1).

Histological analysis of mutant placentas in comparison with littermate controls revealed no abnormalities at E8.0 (supplementary material Fig. S2A,B). Occlusion of the ectoplacental cavity and chorioallantoic attachment occurred normally, resulting in chorionic plates in contact with the ectoplacental cone and allantois at E9.5 (Fig. 2A,B). In control placentas at E9.5, the initially flat chorion began to undergo branching morphogenesis to form the labyrinth, and fetal blood vessels from the allantois started extending into the developing villi (Fig. 2A). By contrast, *Grhl2* mutants showed a marked disruption of chorionic branching, resulting in flat and compact chorionic plates with scant fetal blood vessel ingrowth (Fig. 2B,D) and in reduced thickness of the labyrinth at E10.5 (Fig. 2C,D, arrows). Labeling of fetal blood vessels and maternal blood sinuses in H&E-stained E10.5 sections based on the presence of nucleated (fetal) or non-nucleated (maternal) erythrocytes revealed a complex network of fetal and maternal blood spaces in controls, whereas $Grhl2^{-/-}$ placentas exhibited a marked simplification (Fig. 2E,F). Fetal vasculature, as labeled by PECAM1 staining, largely remained in the allantoic

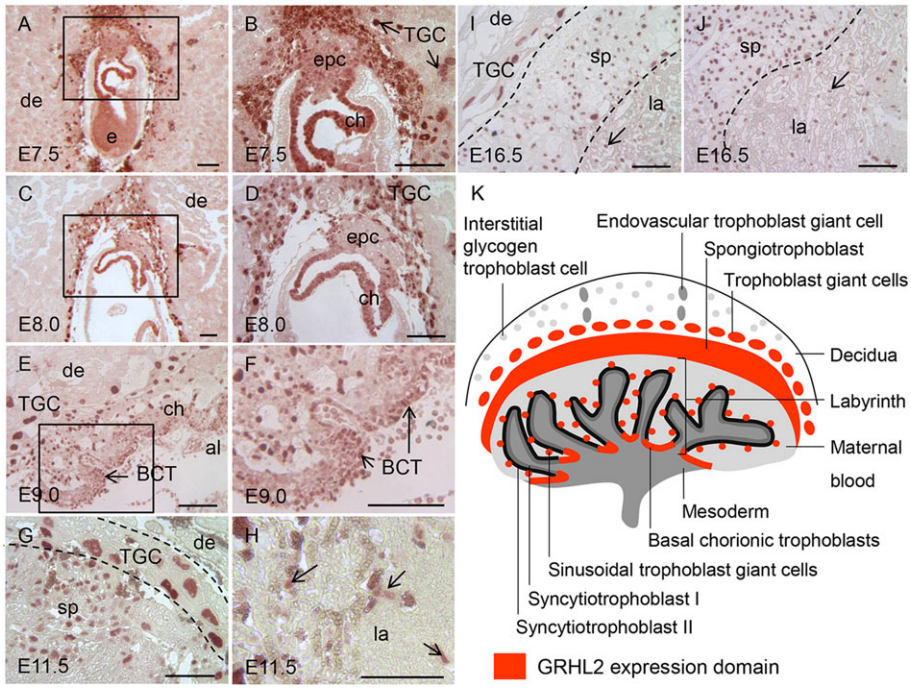

Fig. 1. GRHL2 expression in the wild-type mouse placenta. (A-J) GRHL2 immunohistochemistry revealed its nuclear localization in different trophoblast cell types at E7.5 (A,B), E8.0 (C,D), E9.0 (E,F), E11.5 (G,H) and E16.5 (I,J). Arrows in H-J mark sinusoidal TGCs. al, allantois; BCT, basal chorionic trophoblast; ch, chorion; de, decidua; e, embryo; epc, ectoplacental cone; la, labyrinth; sp, spongiotrophoblast; TGC, trophoblast giant cell(s). Boxed regions in A,C,E are magnified in B,D,F. (K) Schematic of the GRHL2 expression domain in the murine placenta. Scale bars: 100 µm.

Development (2015) 142, 1125-1136 doi:10.1242/dev.113829

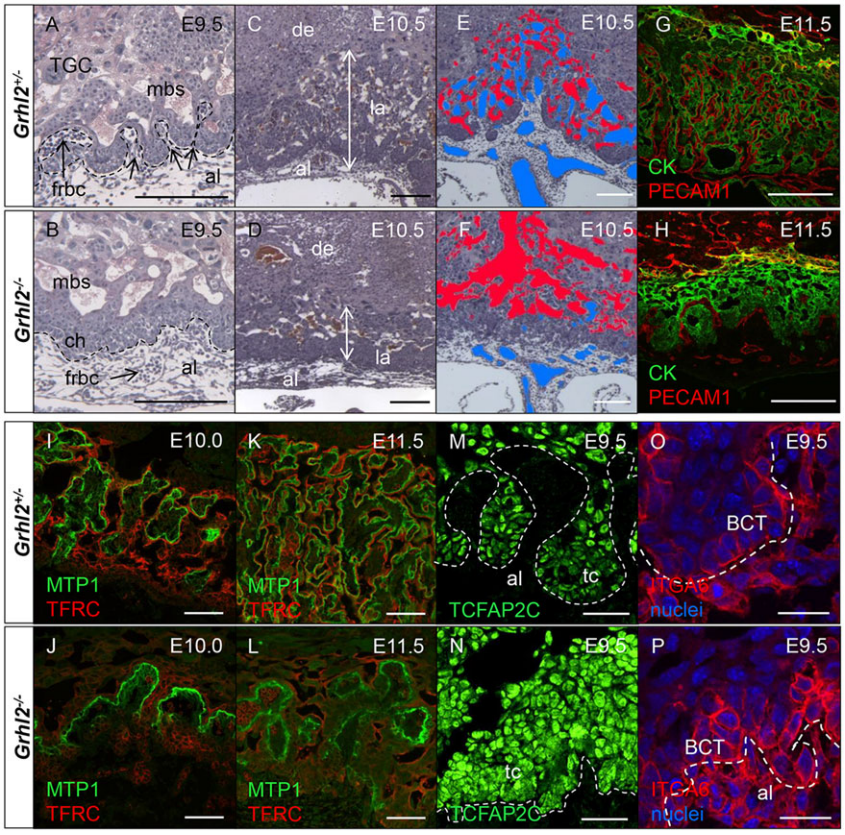

Fig. 2. *Grhl2*$^{-/-}$ placentas show defective trophoblast branching and BCT abnormalities. (A-F) H&E staining of *Grhl2*$^{+/-}$ control and *Grhl2*$^{-/-}$ placentas revealed a disruption of chorion branching and fetal blood vessel permeation in mutants at E9.5 (A,B). *Grhl2*$^{-/-}$ placentas exhibited a compact labyrinth structure with scant blood vessel spaces at E10.5 (C,D). Arrows in C and D indicate a reduced labyrinth thickness. Labeling of fetal (blue) and maternal (red) blood spaces based on the presence of fetal nucleated erythrocytes or maternal non-nucleated erythrocytes revealed defective permeation of fetal blood vessels into the trophoblast layer in E10.5 mutants (F) as compared with littermate controls (E). (G,H) Immunofluorescence staining of pan-cytokeratin (CK, green) and PECAM1 (red) confirmed reduced invasion of fetal blood vessels into the labyrinth and a reduced thickness of this layer in mutants at E11.5. (I-L) Detection of the STB layers by co-staining of the transferrin receptor (TFRC, red; STB I) and ferroportin (MTP1, green; STB II) at E10.0 (I,J) and E11.5 (K,L) revealed that trophoblast branching was initiated in *Grhl2*$^{-/-}$ placentas but that refinement of the feto-maternal barrier was disturbed, resulting in only a few, simplified branches (J,L) as compared with the complex STB compartment of controls (I,K). (M,N) Architectural disorganization of BCT cells in E9.5 *Grhl2*$^{-/-}$ placentas. Trophoblast cells were labeled by TCFAP2C immunostaining. Whereas infolding of BCT cells occurred properly in controls (M), trophoblast cells appeared disorganized in mutants (N). (O,P) Immunofluorescence analysis of integrin alpha 6 (ITGA6) localization revealed abnormal apicobasal polarity in *Grhl2*$^{-/-}$ BCT cells (P) as compared with *Grhl2*$^{+/-}$ controls (O) at E9.5. The dashed line marks the boundary between trophoblasts and allantois. frbc, fetal red blood cells; mbs, maternal blood sinuses; tc, trophoblast cells; for other labels, see Fig. 1. Scale bars: 200 µm in A-F; 250 µm in G,H; 75 µm in I-L; 100 µm in M,N; 25 µm in O,P.

compartment and failed to permeate into the pan-cytokeratin-labeled trophoblast layer (Fig. 2G,H; supplementary material Fig. S2C,D). GRHL2 was not expressed in fetal blood vessels themselves (Fig. 1), suggesting that the reduced fetal vascularization was secondary to defective trophoblast branching. Co-immunostaining of the labyrinth markers transferrin receptor and ferroportin (SLC40A1 – Mouse Genome Informatics), which label STB layer I and II, respectively, demonstrated a progressively complex and expanding STB compartment in controls at E10.0 and E11.5, but markedly defective development in *Grhl2*$^{-/-}$ placentas, with scant evidence of STB differentiation in tip regions (Fig. 2I-L; supplementary material Fig. S2E,F). Although trophoblast branching morphogenesis was initiated, it failed to progress appropriately in mutants (Fig. 2J,L; supplementary material Fig. S2F). Moreover, STB layer II appeared thickened at differentiation sites, as indicated by ferroportin staining (supplementary material Fig. S2G,H). Together, these findings suggest a central role for *Grhl2* in regulating labyrinth trophoblast morphogenesis and differentiation.

We next analyzed trophoblast-specific differentiation markers to determine the presence and quantity of different cell types. To label branch points in the chorionic layer, we stained for *Gcm1* mRNA. As previously reported, control placentas showed *Gcm1* staining in clusters at prospective branching initiation sites at E9.5 and at branch points in the labyrinth at E11.5 (supplementary material Fig. S3A-D) (Anson-Cartwright et al., 2000). In E9.5 *Grhl2*$^{-/-}$ placentas, *Gcm1* was expressed at the sites of branch point initiation (supplementary material Fig. S3B). Consistently, trophoblast branching was initiated in mutants, indicating that the disturbed trophoblast branching was not related to defective *Gcm1* expression. However, mutants contained markedly reduced numbers of *Gcm1*-positive branching initiation sites (supplementary material Fig. S3B,D), indicating a quantitative defect in branch point formation. The spongiotrophoblast marker *Tpbpa* was expressed in mutants (supplementary material Fig. S3E,F). We monitored the development and differentiation of TGC types by staining for specific markers *Prl3d1*, *Prl3b1*, *Prl2c2* and *Hand1* (supplementary material Fig. S3G-N), indicating that several hallmarks of TGC differentiation were unaltered in E9.5 *Grhl2*$^{-/-}$ placentas.

Since these data did not identify substantial defects outside the chorionic trophoblast compartment, we next focused on BCT cells,

Development (2015) 142, 1125-1136 doi:10.1242/dev.113829

which express high levels of GRHL2 and are known to drive chorionic branching. During placentation, BCT cells were initially cuboid and became progressively flattened after allantoic attachment. Labeling with the trophoblast marker TCFAP2C confirmed the ordered appearance of BCT cells in wild-type placentas, but revealed disorganized and multilayered BCT cells in *Grhl2* mutants (Fig. 2M, N). To analyze cell polarity in the BCT cell layer, we stained for integrin alpha 6 (ITGA6), a marker of the basolateral membrane domain. Whereas ITGA6 showed a strictly basolateral pattern in control BCT cells, its positioning appeared randomized in *Grhl2*$^{-/-}$ BCT cells, with cuboid cells that failed to flatten and branch (Fig. 2O, P), indicating a disruption of apicobasal polarization and of cell orientation in mutant BCT cells. Analysis of cell proliferation in the BCT layer via Ki-67 (MKI67) immunofluorescence showed no differences between controls and mutants at E9.5 (see supplementary material Fig. S4A-E). Moreover, we found no evidence for apoptosis in *Grhl2*$^{-/-}$ trophoblasts by activated caspase 3 immunostaining (supplementary material Fig. S4F-M). Hence, the defects observed in *Grhl2*$^{-/-}$ placentas appear to be due to defective cellular morphogenesis in the BCT layer rather than to alterations in proliferation or apoptosis.

Epiblast-specific *Grhl2* deletion rescues placenta defects

Loss of intraplacental GRHL2 could contribute to the profound embryonic phenotype of *Grhl2*$^{-/-}$ mice and might explain lethality after E10.5. However, the severe embryonic alterations in *Grhl2*$^{-/-}$ mice might also aggravate the placenta defects. Thus, we generated a conditional allele of *Grhl2* (*Grhl2*^{flox}) allowing tissue-specific Cre-dependent *Grhl2* ablation (supplementary material Fig. S5A). *Sox2Cre* mice enable Cre-mediated recombination selectively in the epiblast-derived embryo and epiblast-derived extraembryonic membranes, including amnion, yolk sac mesoderm and allantois, as shown in previous studies at E7.5 (Hayashi et al., 2002). We confirmed the absence of *Sox2Cre*-mediated recombination in E9.5 trophectoderm-derived trophoblasts by β-galactosidase staining in *Sox2Cre;R26R-lacZ* placenta sections, which revealed recombination only in the allantoic mesoderm (supplementary material Fig. S5B). We then crossed male *Sox2Cre;Grhl2*$^{+/-}$ with female *Grhl2*$^{flox/flox}$ mice to generate *Sox2Cre;Grhl2*$^{\Delta/-}$ embryos. These embryos were present at Mendelian ratios up to E11.5. Their phenotype was indistinguishable from that of *Grhl2*$^{-/-}$ embryos (Fig. 3A-C; supplementary material Fig. S5C-F) and included split face malformations, exencephaly, as well as anterior and lumbosacral spina bifida. Immunofluorescence staining confirmed the complete absence of GRHL2 protein in all intraembryonic tissues of *Sox2Cre;Grhl2*$^{\Delta/-}$ mice (Fig. 3D-G). H&E-stained E9.5 to E11.5 placenta sections of *Sox2Cre;Grhl2*$^{\Delta/-}$ embryos revealed that, in contrast to *Grhl2*$^{-/-}$ mice, trophoblast branching morphogenesis plus permeation and branching of fetal blood vessels occurred normally. The complex network of fetal blood vessels and maternal blood sinuses developed normally (Fig. 3H-P). Despite the rescue of placental defects, we only recovered *Sox2Cre;Grhl2*$^{\Delta/-}$ embryos up to E11.5, with evidence of IUGR and tissue decay similar to *Grhl2*$^{-/-}$ mice. These data indicate that *Grhl2* in epiblast-derived tissues accounted for intraembryonic defects, but not for the placenta defect, implying a crucial role for *Grhl2* in trophectoderm-derived trophoblast lineages.

Identification of placental GRHL2 target genes by integrated genomic analyses

To understand the molecular basis of placenta defects in *Grhl2*$^{-/-}$ mice, we employed ChIP-sequencing (ChIP-seq) on mouse placenta tissue using a GRHL2 antibody that we had previously shown to be specific (Werth et al., 2010). We identified 5282 peaks ($P<10^{-5}$) of GRHL2 binding across the mouse genome using MACS (Zhang et al., 2008) (Fig. 4 and Fig. 5A). GRHL2 ChIP peaks were clustered around transcriptional units, with the majority located in upstream regulatory regions and introns (Fig. 4A). *De novo* motif discovery within the top 10% of the GRHL2-associated DNA regions (528 peaks) using MEME (Bailey and Elkan, 1994) yielded a sequence (Fig. 4B) identical to previously identified grainyhead binding motifs (Gao et al., 2013). A comparison with known vertebrate transcription factor binding sites using TOMTOM (Gupta et al., 2007) revealed high similarity

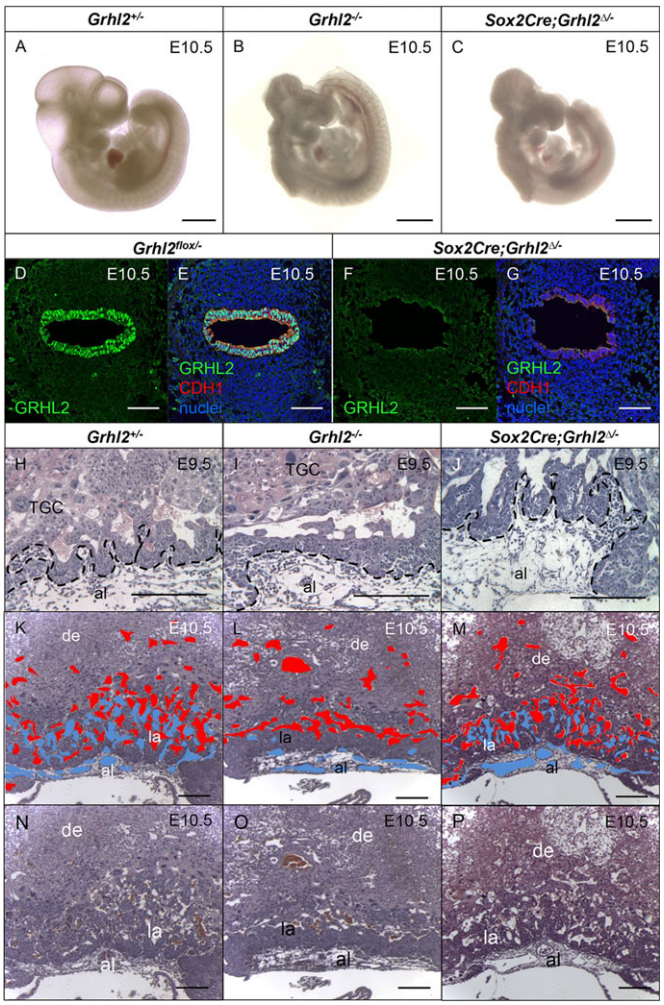

Fig. 3. Selective *Sox2Cre*-mediated *Grhl2* inactivation in epiblast-derived tissues rescues placenta defects of *Grhl2*$^{-/-}$ mice. (A-C) Whole-mount E10.5 control (*Grhl2*$^{+/-}$, A), *Grhl2*$^{-/-}$ (B) and *Sox2Cre;Grhl2*$^{\Delta/-}$ embryos (C). (D-G) Validation of intraembryonic *Grhl2* deletion in *Sox2Cre;Grhl2*$^{\Delta/-}$ embryos. GRHL2 immunostaining on control embryo sections (*Grhl2*$^{flox/-}$, D,E) showed high GRHL2 levels, whereas GRHL2 was absent from all intraembryonic tissues of *Sox2Cre;Grhl2*$^{\Delta/-}$ mice, as shown here for the foregut (F,G). (H-P) H&E-stained placenta sections from control (*Grhl2*$^{+/-}$, H,K,N), global *Grhl2*-deficient (*Grhl2*$^{-/-}$, I,L,O) and *Sox2Cre;Grhl2*$^{\Delta/-}$ (J,M,P) embryos at E9.5 (H-J) and E10.5 (K-P). The dashed lines mark the boundary between trophoblasts and allantois (al). (K-M) Blood spaces with fetal nucleated erythrocytes and maternal non-nucleated erythrocytes are labeled in blue and red, respectively, revealing a defective interaction of fetal and maternal blood in E10.5 *Grhl2*$^{-/-}$ placentas (L), but not in controls (K) or in *Sox2Cre;Grhl2*$^{\Delta/-}$ placentas (M). For labels, see Fig. 1. Scale bars: 1 mm in A-C; 75 µm in D-G; 200 µm in H-P.

Development (2015) 142, 1125-1136 doi:10.1242/dev.113829

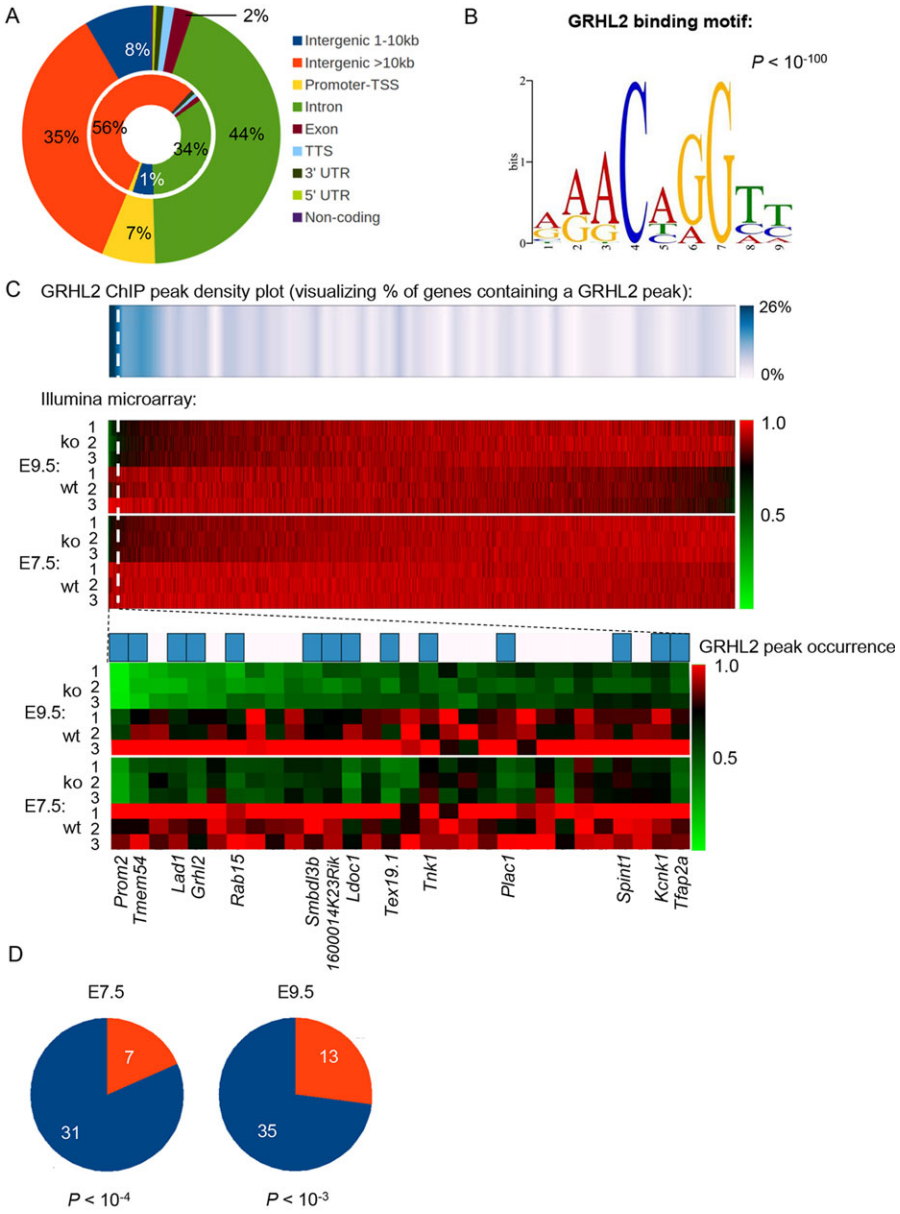

Fig. 4. Integration of ChIP-seq and microarray data identifies a putative placental GRHL2 target gene set. (A) Annotation of GRHL2 ChIP peaks obtained with E17.5 placenta tissue. The majority of GRHL2 peaks were clustered around transcriptional units and in upstream regulatory regions and introns (outer circle). The inner circle represents the annotation of an equal number of random peaks. TSS, transcription start site; TTS, transcription termination site; UTR, untranslated region. (B) *De novo* motif discovery from the top 10% GRHL2 ChIP peaks identified a sequence that is identical to previously published grainyhead binding motifs. *P*-value as provided by MEME. (C) Combination of GRHL2 ChIP peak and gene expression data analysis visualized by heat maps. In the center panel, heat maps are shown for all genes according to Illumina microarray analysis ordered by fold rank in E9.5 wild-type control (wt) versus *Grhl2*$^{-/-}$ (ko) placenta. Each numbered row represents one biological replicate. The dashed lines mark the top 150 genes. Genes at E7.5 are shown beneath in the same order. The GRHL2 peak density plot (top panel) corresponding to the genes shown in the heat maps beneath visualizes an increased frequency of GRHL2 ChIP peak occurrence in the vicinity of genes downregulated in *Grhl2*$^{-/-}$ placentas (linear interpolated density plot over 500 genes). The heat maps at the bottom visualize the intersection of the top 150 fold-ranked genes for E9.5 and E7.5 separately. Blue bars indicate the presence of a GRHL2 ChIP peak near the respective gene. (D) Quantifying GRHL2 peak occurrence in the top 150 downregulated (blue) and upregulated (red) genes revealed a marked enrichment in genes downregulated in mutants (*P*-values calculated using Fisher's exact test).

to the motif recognized by transcription factor CP2-like 1 (TFCP2L1; $P<0.005$), another member of the CP2 family (Chen et al., 2008). GRHL2 binding sites detected in kidney epithelial cells (our unpublished data) compared with our placental GRHL2 peaks showed an overlap of 41%. Moreover, 3611 out of the 5282 GRHL2 ChIP peaks determined in placenta tissue mapped to syntenic regions of the human genome, of which 592 (16.4%) overlapped with GRHL2 binding sites recently identified in lung epithelial cells (Gao et al., 2013).

Moreover, we used microarrays to compare gene expression in *Grhl2*$^{-/-}$ versus control E7.5 and E9.5 placentas (Fig. 4C). The intersection of the top 150 genes downregulated in *Grhl2*$^{-/-}$ placentas at E7.5 and E9.5 yielded 33 genes (supplementary material Table S2). Interestingly, the previously identified embryonic *Grhl2* target genes *Cldn4* and E-cadherin (*Cdh1*) (Werth et al., 2010) were absent from this gene list. This points to a marked tissue specificity of *Grhl2* functions and suggests that the target gene set of *Grhl2* in placenta differs from that in other tissues. Consistently, CLDN4 protein expression analysis by immunofluorescence staining showed high CLDN4 levels in BCT cells compared with the overlying chorionic trophoblasts in controls, and we found no profound effect of *Grhl2* deficiency on placental *Cldn4* expression by *in situ* hybridization as well as immunostaining at E9.5 and E11.5 (supplementary material Fig. S6). As *Cldn4* expression was maintained in BCT cells deficient for *Grhl2*, this suggests that alternative pathways maintain *Cldn4* expression in these cells.

In contrast to the downregulated genes, the intersection of the top 150 genes upregulated in mutants at E7.5 and E9.5 revealed no overlap. In addition, genes downregulated in mutant placentas revealed a marked overrepresentation of GRHL2 peak occurrence in the vicinity of their genomic sequences (±2 kb) when compared with upregulated genes (Fig. 4C,D). These findings suggest that GRHL2 controls transactivation rather than transrepression of target genes in the mouse placenta.

To gain further functional insight, we performed gene ontology analysis using Homer (Heinz et al., 2010) to identify overrepresented functional categories within genes possessing a GRHL2 ChIP peak (within ±2 kb around genomic sequences) and

Development (2015) 142, 1125-1136 doi:10.1242/dev.113829

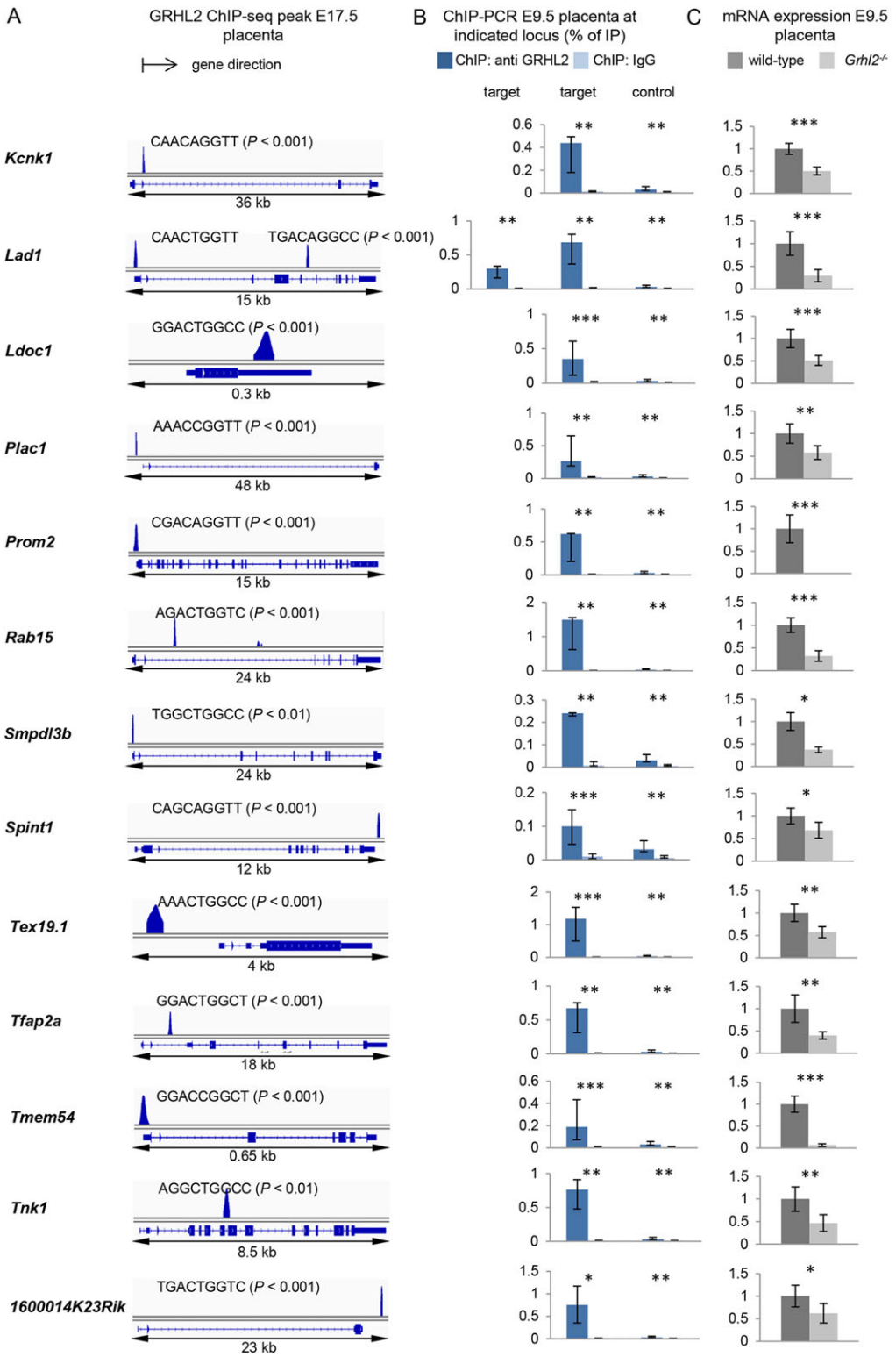

Fig. 5. Identification and validation of putative placental GRHL2-dependent target genes. (A) Depicted are all genes of the putative core target gene set (see Table 1) with a GRHL2 binding peak and showing significant downregulation in *Grhl2*$^{-/-}$ placentas as compared with wild-type controls based on microarray analysis (P<0.05). Peak occurrence and corresponding binding motifs are depicted at genomic loci of all target genes identified by GRHL2 ChIP-seq using E17.5 placenta tissue. ChIP peaks (blue) are visualized using QuEST (Valouev et al., 2008). (B) Validation of GRHL2 ChIP-seq peaks by ChIP with subsequent quantitative PCR analysis performed on E9.5 placenta tissue with normalization for total input. IgG was used as antibody control. Bars represent the median and error bars show the 25th and 75th percentile; n=3 biological replicates. *P<0.05, **P<0.01, ***P<0.001 versus IgG (Mann–Whitney U test). (C) Real-time RT-PCR confirmed significant downregulation of all GRHL2 targets in E9.5 *Grhl2*$^{-/-}$ placentas compared with wild-type controls identified by microarray analysis. β-actin was used as internal standard. Error bars represent mean±s.d.; n=6 biological replicates. *P<0.05, **P<0.01, ***P<0.001 versus wild-type control (Mann–Whitney U test).

within the top 150 genes downregulated in E7.5 and E9.5 *Grhl2*$^{-/-}$ placentas. Both analyses revealed a significant overrepresentation of genes involved in epithelial cell differentiation, epithelial morphogenesis and placenta development (supplementary material Table S3).

To determine a set of putative GRHL2 targets, we identified genes that were among the top 150 downregulated in mutant placentas at E7.5 and E9.5 and displayed a GRHL2 binding peak within a ±2 kb region around the gene. This yielded a module of 13 putative placental GRHL2 core targets (Fig. 4C,E, Fig. 5A, Table 1). ChIP-PCR using E9.5 placenta tissue confirmed specific enrichment at the putative GRHL2 binding areas of all 13 target genes when compared with the IgG control, and thus confirmed GRHL2 binding peaks identified by ChIP-seq (Fig. 5B). Validation of expression differences by quantitative PCR confirmed a significant downregulation of

Development (2015) 142, 1125-1136 doi:10.1242/dev.113829

Table 1. Core set of GRHL2-dependent genes

Gene	Fold change microarray E7.5	Fold change microarray E9.5	Peak location
Kcnk1	1.3	1.8	Intron 1
Lad1	1.5	2.7	TSS, intron 4
Ldoc1	1.9	1.8	3′ UTR
Plac1	1.9	1.7	–1134 bp
Prom2	3.2	11.0	TSS
Rab15	1.9	2.4	Intron 1
Smpdl3b	1.5	1.9	TSS
Spint1	1.3	1.5	+63 bp
Tex19.1	2.0	1.8	–736 bp
Tfap2a	1.9	1.6	Intron 1
Tmem54	2.0	4.7	TSS
Tnk1	1.2	1.7	Intron 6
1600014K23Rik	1.4	1.9	+1615 bp

Intersection of the top 150 fold-ranked downregulated genes (wild-type control versus *Grhl2*$^{-/-}$) at E7.5 and E9.5 with additional GRHL2 peak occurrence yielded a set of 13 potential GRHL2 core targets. Peak location (bp) is relative to gene body.

all 13 genes in E9.5 mutant placentas (Fig. 5C). A literature search revealed that homozygous knockouts for *Spint1* (Tanaka et al., 2005), *Plac1* (Jackman et al., 2012), *Tex19.1* (Tarabay et al., 2013), *Kcnk1* (Millar et al., 2006), *Tfap2a* (Schorle et al., 1996; Zhang et al., 1996) and *Prom2* (Tang et al., 2010) had been phenotypically characterized previously, with three, namely *Spint1*, *Plac1* and *Tex19.1*, displaying a placenta phenotype. Whereas *Plac1*$^{-/-}$ and *Tex19.1*$^{-/-}$ mice exhibit milder placenta defects that manifest in late pregnancy (Jackman et al., 2012; Tarabay et al., 2013), *Spint1*$^{-/-}$ mice have been reported to display an early placenta defect with lethality at E10.5 (Tanaka et al., 2005; Fan et al., 2007; Szabo et al., 2007), similar to the phenotype we found in *Grhl2*$^{-/-}$ mice.

Grhl2$^{-/-}$ placentas display phenotypic hallmarks of *Spint1* deficiency

Spint1 encodes a cell membrane-associated Kunitz type 1 serine protease inhibitor (Shimomura et al., 1997) that is expressed in several epithelial cells and tissues, including the placenta, kidney and intestine (Kataoka et al., 2000; Yamauchi et al., 2004; Oberst et al., 2005; Szabo et al., 2007; Kawaguchi et al., 2011). Similar to *Grhl2*$^{-/-}$ placentas, chorionic trophoblasts of *Spint1*$^{-/-}$ placentas fail to establish a labyrinth, fetal vascularization is absent, and the trophoblast layer appears to be compact (Tanaka et al., 2005; Fan et al., 2007; Szabo et al., 2007). Moreover, SPINT1 is expressed at high levels in BCT cells in E9.5 placentas (Tanaka et al., 2005; Fan et al., 2007; Szabo et al., 2007). Interestingly, the *Spint1* gene featured a GRHL2 ChIP peak at the 3′ end in a region that contains the grainyhead consensus motif CAGCAGGTT (Fig. 5A) and that displayed histone H3 lysine 4 monomethylation (H3K4me1) and histone H3 lysine 27 acetylation (H3K27ac) in mouse placenta, two histone modifications characteristic of active enhancers (based on mouse placenta ENCODE data, not shown).

Together, these data suggest that GRHL2 might serve to ensure high *Spint1* expression levels in BCT cells. The downregulation of *Spint1* mRNA in total placenta extracts of *Grhl2*-deficient mice was relatively mild (Fig. 5C). However, this might reflect a dilution of the cell-specific effect in BCT cells, since *Spint1* is expressed at high levels in BCT cells and at lower levels in surrounding trophoblasts. To assess the effect of *Grhl2* deletion on *Spint1* expression in BCT cells, we localized *Spint1* mRNA and protein in the placenta. *Spint1* mRNA expression, as detected by *in situ* hybridization, showed a high level of *Spint1* mRNA in BCT cells of wild-type placentas. In *Grhl2*-deleted placentas, *Spint1* mRNA was specifically reduced in BCT cells compared with controls (Fig. 6A-D). Next, we carried out immunofluorescence staining using a SPINT1 antibody, confirming high cell membrane-associated SPINT1 levels in BCT cells of control placentas with markedly lower expression in other trophoblast layers (Fig. 6E; supplementary material Fig. S7A,B). By contrast, BCT cells of *Grhl2*$^{-/-}$ placentas showed strongly reduced SPINT1 protein expression, which was at levels indiscernible from that in other surrounding cell types (Fig. 6F; supplementary material Fig. S7C,D). We quantitatively estimated SPINT1 immunofluorescence intensity in *Grhl2*-deficient versus control BCT cells and overlying chorionic trophoblast cells using software-assisted (ImageJ) image analysis. This revealed a specific and significant (P<0.001) reduction of SPINT1 immunofluorescence intensity in the BCT cells of *Grhl2*$^{-/-}$ placentas, which resembled the weaker staining intensity of surrounding trophoblasts (Fig. 6G). These results supported the hypothesis that GRHL2 functions to enhance *Spint1* expression levels in BCT cells.

Spint1$^{-/-}$ mice have been shown to exhibit reduced *Cdh1* expression in BCT cells as well as basement membrane defects, including fragmented laminin deposition and disrupted basement membranes at the chorioallantoic interface adjacent to the BCT layer (Fan et al., 2007; Szabo et al., 2007). We analyzed E9.5 *Grhl2*$^{-/-}$ placentas for these phenotypic hallmarks of *Spint1* deficiency. In wild-type placentas the BCT cells formed a single compact epithelial-like cell layer and expressed high levels of CDH1, which lined cell junctions. By contrast, in *Grhl2*-deleted BCT cells CDH1 expression was strongly reduced (Fig. 6H,I). Immunofluorescence staining for the basement membrane markers laminin and collagen IV revealed continuous basement membranes at the chorioallantoic interface lining the basal surface of BCT cells in controls (Fig. 6J,L), whereas in *Grhl2* mutants the basement membranes were fragmented and appeared at atypical positions relative to the BCT cell layer (Fig. 6K,M). Transmission electron microscopy confirmed the fragmentation and thinning of basement membranes in *Grhl2*$^{-/-}$ placentas (Fig. 6N-Q).

Each of these phenotypes was strongly reminiscent of that reported in *Spint1*$^{-/-}$ placentas, consistent with the hypothesis that they are caused by the reduction of SPINT1 expression in *Grhl2*$^{-/-}$ placentas. Importantly, immunostaining showed that SPINT1 (supplementary material Fig. S8A,B), CDH1 (supplementary material Fig. S8C,D) and laminin and collagen IV (supplementary material Fig. S8E-H) expression levels and distribution patterns were normal in BCT cells of *Sox2Cre;Grhl2*$^{\Delta/-}$ placentas, excluding an effect of extraplacental GRHL2 in the above phenotypes.

Evidence for conserved GRHL2 expression and activity

To determine the potential relevance of *GRHL2* and its target gene set in human placentation, we examined GRHL2 expression in human placentas by immunohistochemistry (Fig. 7A-E). GRHL2 was predominantly expressed in human villous cytotrophoblasts, but also in some STB cells of primary stem villi adjacent to the chorionic plate and in distal villi (Fig. 7A). GRHL2 expression in human villous cytotrophoblasts was reminiscent of the pattern in mouse BCT cells. Moreover, GRHL2 was present in invasive extravillous trophoblasts and in cytotrophoblast cell columns (Fig. 7B,C). During later pregnancy, GRHL2 was present at high levels also in most STB cells. No GRHL2 staining was observed in the mesenchymal cells of the villous stroma or in vascular cells (Fig. 7D,E).

Development (2015) 142, 1125-1136 doi:10.1242/dev.113829

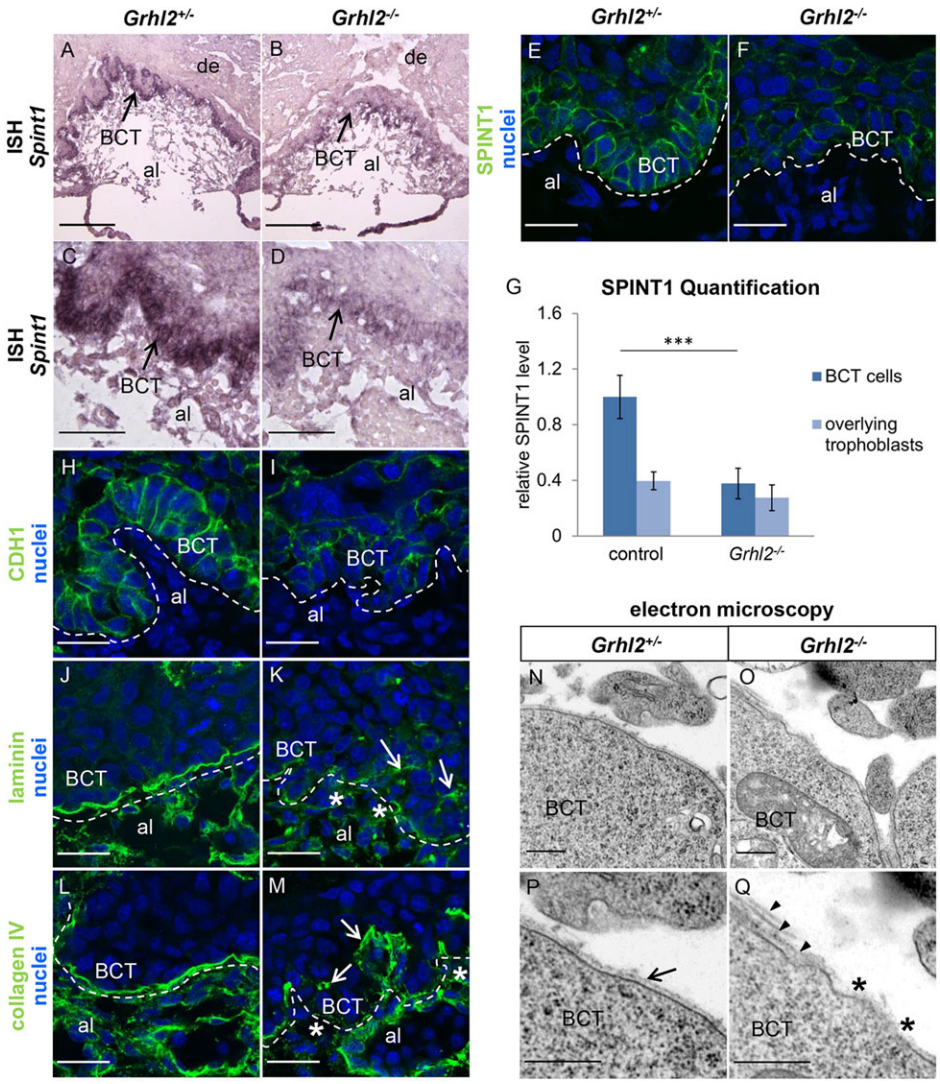

Fig. 6. GRHL2 regulates SPINT1 expression, cellular polarity and basement membrane integrity in BCT cells. (A-F,H-M) *Spint1*/SPINT1 (A-F) and CDH1 (H,I) expression levels as well as laminin (J,K) and collagen IV (L,M) deposition are defective in BCT cells at the chorioallantoic interface (dashed lines) in placentas of *Grhl2*$^{-/-}$ embryos (B,D,F,I,K,M) compared with control *Grhl2*$^{+/-}$ placentas (A,C,E,H,J,L). (K,M) Arrows indicate atypical laminin and collagen IV deposition, and asterisks indicate basement membrane ruptures. (G) Quantification and comparison of SPINT1 fluorescence intensity of BCT cells and overlying chorionic trophoblast cells in control versus *Grhl2*$^{-/-}$ placentas. Relative intensities were calculated from mean gray values determined for BCT cells and overlying trophoblast cells using ImageJ. Error bars represent mean±s.d. ***P<0.001 for control versus *Grhl2*$^{-/-}$ (Mann–Whitney *U* test). (N-Q) Transmission electron microscopy of E9.5 placentas confirmed basement membrane ruptures at the chorioallantoic interface in mutants, as indicated by areas of lower electron density (Q, asterisks) and disorganized deposits (Q, arrowheads). The arrow (P) indicates the basement membrane; for other labels, see Fig. 1. Scale bars: 75 µm in A-D; 25 µm in E,F,H-M; 500 nm in N-Q.

We next analyzed the placental expression domain of human homologs of the *Grhl2* target gene set using publicly available high-quality immunohistochemistry data deposited in the Human Protein Atlas Project (Uhlen et al., 2010). To avoid the detection of non-specific staining, we limited the analysis to antibodies with supportive western blot data and medium or high staining in placentas based on Protein Atlas scoring, which were available for KCNK1, RAB15, LAD1 and TFAP2A. Remarkably, each of these proteins was co-expressed with GRHL2 in villous cytotrophoblasts and STB cells (supplementary material Fig. S9).

Additionally, based on publically deposited microarray data from 34 human placenta samples (Huuskonen et al., 2008; Mikheev et al., 2008; Founds et al., 2009), human orthologs of GRHL2 and its target genes showed a statistically significant co-regulation (P<0.01; Fig. 7F). Within the target gene set, *SPINT1* expression displayed one of the highest correlations with *GRHL2* (r=0.94). To further substantiate their co-regulation, we analyzed *GRHL2* and *SPINT1* mRNA expression in 84 human villous placenta samples by quantitative PCR and found a high level of correlation across all samples (r=0.77, P<10^{-6}; Fig. 7G). Immunohistochemistry confirmed previously reported data that SPINT1 is highly expressed in villous cytotrophoblasts of primary stem villi and more distal villi (Fig. 7H,I) (Hallikas et al., 2006). Collectively, these data suggest that the *Grhl2*-dependent target gene set that we identified in mouse is conserved in human placentation. The findings also indicate that *GRHL2* targets a villous cytotrophoblast signature and are consistent with the notion that human villous cytotrophoblasts share functional characteristics with BCT cells in mice.

DISCUSSION

Our findings indicate that *Grhl2* is essential for normal placental development as well as for appropriate gene regulation and differentiation of BCT cells of the placental labyrinth. GRHL2 transcriptionally activates regulators of placental development and epithelial morphogenesis, including *Spint1*, which encodes the serine protease inhibitor Kunitz type 1 that regulates BCT cell integrity and labyrinth formation. *Spint1* might mediate some of the effects of GRHL2, since *Grhl2*-deficient placentas displayed characteristic hallmarks of *Spint1* deficiency. In human placentas, orthologs of GRHL2 and its targets displayed co-regulation, suggesting conservation of the *Grhl2*-coordinated gene network and that these genes might participate in syndromes of placental dysfunction.

This is the first report to identify a role of *Grhl2* in placenta development and in branching morphogenesis in general. In

Development (2015) 142, 1125-1136 doi:10.1242/dev.113829

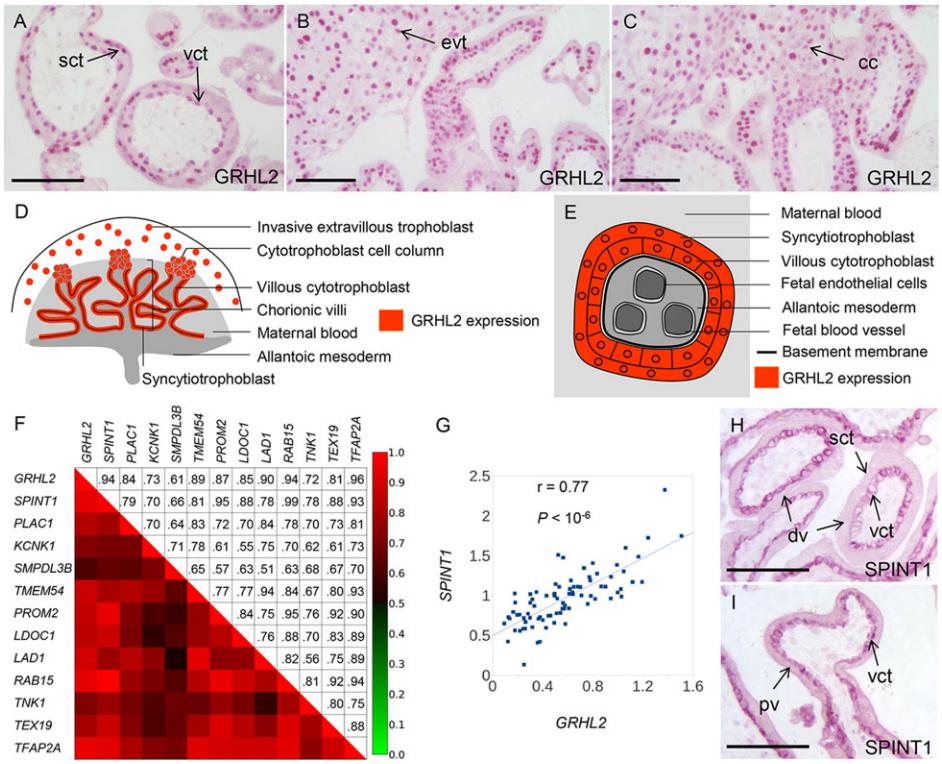

Fig. 7. *GRHL2* and its putative target gene set in human placentation. (A-C) In human placentas, GRHL2 is detected by immunohistochemistry in villous cytotrophoblasts (vct), syncytiotrophoblasts (sct), cytotrophoblast cell columns (cc) and invasive extravillous trophoblasts (evt). (D,E) Schematic of the human placenta (D) and a transverse section of a human chorionic villus (E) showing the GRHL2 expression domain. (F) Co-regulation of genes from the *Grhl2*-dependent target gene set in human placentas. Shown is the expression correlation matrix and a heatmap visualization for *GRHL2* and twelve target gene orthologs (no human ortholog is known for *1600014K23Rik*) based on publicly available microarray data of 34 human placenta samples. Pearson correlation coefficient calculations between the expression of *GRHL2* and its targets revealed tight co-regulation (P<0.01). (G) Correlation analyses between the expression of *GRHL2* and *SPINT1* as determined by real-time RT-PCR in 84 normal and diseased human villous placenta samples revealed a high level of correlation across all samples (r=0.77, ***P<10^{-6}). (H,I) SPINT1 is detected by immunohistochemistry in the villous cytotrophoblasts of primary (pv) and distal (dv) villi. Scale bars: 100 µm.

addition, we identify genome-wide direct and indirect targets of *Grhl2*, which are enriched in genes encoding regulators of epithelial morphogenesis and placenta development. Our data support the hypotheses that GRHL2 acts to transactivate, rather than to transrepress, these target genes and functions to enhance SPINT1 levels in BCT cells, thereby ensuring BCT layer integrity. Moreover, our results indicate that human villous cytotrophoblasts express human orthologs of GRHL2 and several of its targets, lending further support to the concept that these cells exhibit cellular and molecular similarities with mouse BCT cells.

Grhl2 is expressed in several trophoblast cell types, including BCT cells, spongiotrophoblasts and TGCs. In *Grhl2*$^{-/-}$ placentas, each of these cell types lacks *Grhl2* expression, complicating the interpretation of their relative contribution to the phenotype. Several pieces of evidence suggest that *Grhl2* deletion in BCT cells is primarily responsible for the branching phenotype observed. First, BCT cells are known to be central initiators of labyrinth branching morphogenesis, and these cells exhibit defects in cell polarity, basement membrane deposition, and *Spint1* and *Cdh1* expression following *Grhl2* deletion. It is known that the interaction of the basement membrane component laminin with cell surface integrin receptors of the adjacent epithelium is crucial in the regulation of three-dimensional epithelial morphogenesis (Klein et al., 1988; Sorokin et al., 1990; Durbeej and Ekblom, 1997). Importantly, previous studies have revealed that structural defects of basement membranes at the chorioallantoic interface of collagen IV (*Col4a1*/*Col4a2*)-mutant mice resulted in impaired placental labyrinth formation (Pöschl et al., 2004). Moreover, disruption of *Cdh1* expression is associated with defective labyrinth development (Stemmler and Bedzhov, 2010). Thus, the defects of BCT cells in *Grhl2* mutants reasonably explain the observed failure of labyrinth formation. By contrast, *Grhl2* mutants initially displayed normal spongiotrophoblast and TGC formation based on marker gene expression analysis. Furthermore, *Spint1* displays high expression levels only in BCT cells, but not in other trophoblast cell types, and its expression is strongly reduced only in BCT cells of *Grhl2* mutants. Together, these results suggest that *Grhl2* activity in BCT cells is crucial for labyrinth morphogenesis. However, we cannot exclude additional defects in other trophoblast cell types that might in part be obscured by the early and severe placenta phenotype of mutants. *Grhl2* deletion in specific trophoblast cell types would be required to clarify the cell type-specific effects of *Grhl2* in more detail.

As outlined above, several pieces of evidence support the notion that *Spint1* deficiency contributes to the placental phenotype of *Grhl2*$^{-/-}$ mice. However, ultimate proof of a crucial role of *Spint1* downstream of *Grhl2* is lacking, as it would require a rescue of *Spint1* expression or genetic interference with the *Spint1*/prostasin/matriptase cascade in a *Grhl2*$^{-/-}$ setting, for example by additionally deleting *Prss8* or *St14* (Lin et al., 1999; Szabo et al., 2007, 2012). Both, *GRHL2* and *SPINT1* are expressed in human villous cytotrophoblasts (Shimomura et al., 1997; Kataoka et al., 2000; Wilanowski et al., 2002; Fan et al., 2006; Hallikas et al., 2006; Szabo et al., 2007). Similar to BCT cells, the villous cytotrophoblasts are in direct contact with the basement membrane that separates them from mesodermal fetal stroma and blood vessels. Defects of trophoblast differentiation and morphogenesis are linked with pregnancy-associated diseases. Together with our finding that the expression of *GRHL2* and that of its target genes (including *SPINT1*) are closely correlated in human placenta specimens, this raises the possibility of an involvement of *GRHL2* and its target gene set in human placentation, a hypothesis that merits future detailed analyses.

A comparison of our GRHL2 ChIP-seq data with GRHL2 ChIP-seq data recently generated using primary human airway lung epithelial cells in culture (Gao et al., 2013) and kidney epithelial cells (mIMCD-3; our unpublished data) showed a peak overlap of 17.2% and 41%, respectively. Our findings suggest that GRHL2 controls a set of genes that are generally important for epithelial cell development and thus are common for different cell types or tissues,

Development (2015) 142, 1125-1136 doi:10.1242/dev.113829

but at the same time identify placenta-specific GRHL2 targets in mice. Consistently, ontology analysis of genes with GRHL2 binding peaks revealed a substantial overrepresentation of genes involved in epithelial cell development and morphogenesis and placenta development. Our finding that GRHL2 preferentially associates with genes that are downregulated in *Grhl2*$^{-/-}$ placentas, but not with those that are upregulated, provides *in vivo* evidence that GRHL2 might preferentially activate rather than repress the transcription of its direct target genes.

We have previously identified *Cdh1* as an embryonic GRHL2 target and provided evidence for a direct mechanism of regulation through association of GRHL2 with intron 2 of *Cdh1* (Werth et al., 2010). Although GRHL2 binding to *Cdh1* intron 2 has been confirmed in several studies using ChIP on epiblast-derived cell types (Werth et al., 2010; Varma et al., 2012; Gao et al., 2013), we failed to detect GRHL2 binding at the *Cdh1* locus in placenta tissues. Furthermore, a previous study has shown that *Cdh1* intron 2 sequences are dispensable for *Cdh1*-specific reporter gene expression in extraembryonic, but not intraembryonic, tissues (Stemmler et al., 2005). Together, these findings suggest that *Cdh1* expression in extraembryonic trophoblast cells occurs independently of GRHL2 association with intron 2 and instead might involve GRHL2-dependent regulation of *Spint1*. These ideas require confirmation in future studies.

The expression of *Cldn4*, as another previously identified embryonic GRHL2 target (Werth et al., 2010), was analyzed in whole placental extracts and in BCT cells. *Cldn4* was robustly expressed in BCT cells, as detected by *in situ* hybridization and immunofluorescence staining, but we found no profound effect of *Grhl2* deficiency on placental *Cldn4* expression. Consistently, *Cldn4* was not represented within the *Grhl2* core target set that we identified by integrating comparative microarray analysis of control versus *Grhl2* mutant placentas and ChIP-seq. This points to alternative pathways maintaining *Cldn4* expression in BCT cells.

Thus, neither *Cldn4* nor *Cdh1* seems to be a direct *Grhl2* target gene in BCT cells of the mouse placenta. This argues for a marked tissue specificity of *Grhl2* functions and suggests that the target gene set of *Grhl2* in the placenta differs from that in other tissues.

Placentas from globally *Grhl2*-deficient mice displayed a specific defect of labyrinth formation that was not seen in placentas from mice with an epiblast-specific deletion of *Grhl2*. However, epiblast-specific *Grhl2* deletion failed to rescue embryonic lethality, indicating that intraembryonic *Grhl2* is essential for survival past E11.5. The cause of this lethality is currently unknown. Defects of neural tube closure are normally consistent with survival to later stages of embryonic development. Mice with the mutant allele *Grhl2*^{1Nisw} (Pyrgaki et al., 2011) have been reported to occasionally survive to E18.5 and then display heart defects, with a thinning of the ventricular walls and expansion of the ventricles. Hence, it appears possible that heart defects might have contributed to the embryonic lethality of *Sox2Cre;Grhl2*$^{\Delta/-}$ mice, but we have not analyzed this in detail. Defects in other vascular and hematopoietic lineages could also potentially explain the embryonic lethal phenotype.

The severe placental defects in *Grhl2*-deficient mice are likely to eventually compromise embryonic development; for example, knockout of *Rbm15* or *Socs3* manifests placental defects of somewhat comparable severity to those of *Grhl2* mutants (Takahashi et al., 2003; Raffel et al., 2009). In these mice, the progressive placental defects are associated with embryonic death starting at E10.5. When placental defects are rescued, they survive to birth. Since epiblast-specific deletion of *Grhl2* rescued placental development, but not embryonic survival, we cannot definitively prove the requirement for placental *Grhl2* in maintaining embryonic survival. This would require placenta-specific deletion of *Grhl2*. We attempted to generate *Grhl2*-deficient tetraploid blastocysts in order to carry out tetraploid complementation with wild-type embryonic stem cells. However, we were unable to achieve this because tetraploid blastocysts generated from embryos originating from intercrosses of *Grhl2*$^{+/-}$ mice, regardless of genotype, failed to efficiently support embryonic development.

We believe that our findings may have translational implications, as we have pursued a clinical line of investigation including human samples, and will be of relevance to placental biologists and to researchers exploring the mechanisms and consequences of placental malfunction.

MATERIALS AND METHODS

Animals

Generation of the *Grhl2*-deficient alleles *Grhl2*^{lacZ1} and *Grhl2*^{lacZ4} has been described (Werth et al., 2010). Mice with conditional *Grhl2* alleles were obtained from embryonic stem cells containing a *Grhl2* gene with exon 4 flanked by two loxP sites (supplementary material Fig. S5A). Breeding of female *Grhl2*$^{flox/flox}$ mice with *Grhl2*$^{+/-}$ males carrying the *Sox2Cre* transgene (*Sox2Cre;Grhl2*$^{+/-}$) generated *Sox2Cre;Grhl2*$^{\Delta/-}$ mice (Hayashi et al., 2002). For further details, see supplementary material methods and Tables S4 and S5.

Human tissue samples

We included non-labored placenta samples from complicated and uncomplicated pregnancies delivered by elective Cesarean section at Oslo University Hospital, Oslo, Norway, to analyze the expression correlation of *GRHL2* and *SPINT1*. Details are provided in the supplementary material methods.

Electron microscopy

The fixation and imaging of E9.5 placentas are described in the supplementary material methods.

Immunofluorescence staining

Tissues were fixed in PBS containing 4% paraformaldehyde for 1 h at 4°C and embedded in Tissue-Tek O.C.T. Compound (Sakura Finetek) for cryosectioning. Primary antibodies were incubated overnight at 4°C. For further details of immunofluorescence staining, including antibodies, confocal microscopy and analysis of fluorescence intensity, see the supplementary material methods.

GRHL2 immunohistochemistry

Immunohistochemistry was performed using the EnVision System-HRP (AEC) Kit for rabbit primary antibodies (DakoCytomation). For details, see the supplementary material methods.

In situ hybridization

In situ hybridization on placenta tissue sections was carried out as described in the supplementary material methods and Table S6.

RNA extraction, cDNA synthesis and real-time PCR

Total RNA was isolated using the RNeasy Mini Kit (Qiagen) and cDNA synthesis was performed with the RevertAid First-Strand cDNA Synthesis Kit (Fermentas). Real-time PCR was performed using MESA GREEN qPCR MasterMix Plus for SYBR Assay Rox (Eurogentec) and primers at 200 nM final concentration each. For primer sequences and further details, see the supplementary material methods and Tables S7 and S8.

Microarray analysis

Differential gene expression was examined by Illumina Mouse WG-6 v2.0 Expression Bead Chip microarray analysis. The extraembryonic trophectoderm-derived tissues (chorion, ectoplacental cone and giant cell layer) at E7.5 and the visually identified placentas at E9.5 were separated from embryonic tissue and maternal uterus tissue.

Development (2015) 142, 1125-1136 doi:10.1242/dev.113829

The publicly available human placenta data were downloaded from GEO under accession numbers GSE9984, GSE12767 and GSE7434 (Huuskonen et al., 2008; Mikheev et al., 2008; Founds et al., 2009). For details of the microarray and data analysis, see the supplementary material methods.

ChIP

Twenty-five C57BL/6 E17.5 mouse placentas were harvested, maternal uterus tissue was removed and placentas were pooled. Cross-linking was performed with 1% formaldehyde in PBS for 15 min at room temperature. Chromatin was fragmented to an average size of 300-500 bp by sonication. 100 µg chromatin and 5 µg GRHL2 antibody or isotype control antibody (rabbit IgG) as background control were used per assay using a Chromatin Immunoprecipitation Assay Kit (Upstate, Millipore) according to the manufacturer's protocol. For ChIP-PCR, nine E9.5 placentas were harvested, pooled and cross-linked with 1% formaldehyde for 20 min at room temperature. Sonication of chromatin produced DNA fragments of average size 200-300 bp. 25 µg chromatin and 6 µg GRHL2 antibody or rabbit IgG as background control were used per assay according to established protocols (Li et al., 2003; Schmidt et al., 2009).

ChIP-seq

Complex-associated DNA fragments were de-cross-linked and subjected to a standardized ChIP-sequencing pipeline (Solexa). Libraries of 250-350 bp were prepared according to standard Illumina protocols. For details of the ChIP-seq data analysis, see the supplementary material methods. Microarray and ChIPseq data are available at GEO under the accession numbers GSE65963 (reference series), GSE65960 (microarray data) and GSE65962 (ChIPseq data).

Acknowledgements

We thank Prof. Dr Carmen Birchmeier, Prof. Dr Friedrich C. Luft and Prof. Dr Walter Birchmeier (MDC, Berlin) for critical suggestions regarding the manuscript; Dr Francesca Spagnoli (MDC, Berlin) for providing antibodies; Prof. Dr James C. Cross (University of Calgary), Dr Mateusz Kolanczyk (MPI for Molecular Genetics, Berlin) and Dr Valerie Begay-Mueller (MDC, Berlin) for providing *in situ* probes; Dr Anje Sporbert and Dr Zoltan Cseresnyes (MDC Advance Light Microscopy Facility), Dr Ralf Kühn (MDC Transgene Core Facility), Dr Wei Chen (MDC/BIMSB Next Generation Sequencing Facility); and Antje Sommer, Tatjana Luganskaja, Gabriel Kirchgraber and Siegrun Blauhut (MDC, Berlin) for excellent technical support.

Competing interests

The authors declare no competing or financial interests.

Author contributions

K.M.S.-O. and K.W. designed the project. K.W. performed most of the experiments, with the support of E.Pö., M.W., A.A., M.B. and E.P. C.H. and C.D. performed integrated bioinformatic analyses. K.M.S.-O. and K.W. wrote the paper with inputs from C.H. E.K. provided human placenta tissue and Z.Y.Y. performed immunostaining on human tissue. B.P. performed electron microscopy. R.D., N.H. and A.C.S. provided human placenta samples and performed *Grhl2* and *Spint1* expression analysis by real-time PCR. A.Q., J.B. and M.W. helped with the generation of the conditional *Grhl2* allele. S.V., R.M. and D.W. helped with ChIP-seq data analysis and data interpretation.

Funding

This work was funded by the German Research Foundation [Emmy-Noether grant; Research Unit 667 grant and Research Unit 1368 grant (all to K.M.S.-O.); Research grant DE 631/9-1 (to R.D.)]; and by the Urological Research Foundation (Stiftung Urologische Forschung). R.J.M. was supported by intramural funds [1Z01DC000039-14] from the National Institute on Deafness and Other Communication Disorders, National Institutes of Health (NIDCD/NIH) to Thomas B. Friedman. Deposited in PMC for release after 12 months.

Supplementary material

Supplementary material available online at
http://dev.biologists.org/lookup/suppl/doi:10.1242/dev.113829/-/DC1

References

Adamson, S. L., Lu, Y., Whiteley, K. J., Holmyard, D., Hemberger, M., Pfarrer, C. and Cross, J. C. (2002). Interactions between trophoblast cells and the maternal and fetal circulation in the mouse placenta. *Dev. Biol.* **250**, 358-373.

Anson-Cartwright, L., Dawson, K., Holmyard, D., Fisher, S. J., Lazzarini, R. A. and Cross, J. C. (2000). The glial cells missing-1 protein is essential for branching morphogenesis in the chorioallantoic placenta. *Nat. Genet.* **25**, 311-314.

Auden, A., Caddy, J., Wilanowski, T., Ting, S. B., Cunningham, J. M. and Jane, S. M. (2006). Spatial and temporal expression of the Grainyhead-like transcription factor family during murine development. *Gene Expr. Patterns* **6**, 964-970.

Bailey, T. L. and Elkan, C. (1994). Fitting a mixture model by expectation maximization to discover motifs in biopolymers. *Proc. Int. Conf. Intell. Syst. Mol. Biol.* **2**, 28-36.

Bray, S. J. and Kafatos, F. C. (1991). Developmental function of Elf-1: an essential transcription factor during embryogenesis in Drosophila. *Genes Dev.* **5**, 1672-1683.

Brouns, M. R., De Castro, S. C. P., Terwindt-Rouwenhorst, E. A., Massa, V., Hekking, J. W., Hirst, C. S., Savery, D., Munts, C., Partridge, D., Lamers, W. et al. (2011). Over-expression of Grhl2 causes spina bifida in the Axial defects mutant mouse. *Hum. Mol. Genet.* **20**, 1536-1546.

Chen, X., Xu, H., Yuan, P., Fang, F., Huss, M., Vega, V. B., Wong, E., Orlov, Y. L., Zhang, W., Jiang, J. et al. (2008). Integration of external signaling pathways with the core transcriptional network in embryonic stem cells. *Cell* **133**, 1106-1117.

Cox, B., Kotlyar, M., Evangelou, A. I., Ignatchenko, V., Ignatchenko, A., Whiteley, K., Jurisica, I., Adamson, S. L., Rossant, J. and Kislinger, T. (2009). Comparative systems biology of human and mouse as a tool to guide the modeling of human placental pathology. *Mol. Syst. Biol.* **5**, 279.

Cross, J. C., Baczyk, D., Dobric, N., Hemberger, M., Hughes, M., Simmons, D. G., Yamamoto, H. and Kingdom, J. C. P. (2003a). Genes, development and evolution of the placenta. *Placenta* **24**, 123-130.

Cross, J. C., Simmons, D. G. and Watson, E. D. (2003b). Chorioallantoic morphogenesis and formation of the placental villous tree. *Ann. N. Y. Acad. Sci.* **995**, 84-93.

Durbeej, M. and Ekblom, P. (1997). Dystroglycan and laminins: glycoconjugates involved in branching epithelial morphogenesis. *Exp. Lung Res.* **23**, 109-118.

Egbor, M., Ansari, T., Morris, N., Green, C. J. and Sibbons, P. D. (2006). Morphometric placental villous and vascular abnormalities in early- and late-onset pre-eclampsia with and without fetal growth restriction. *BJOG* **113**, 580-589.

Fan, C. B., He, J. L., Wang, Y. X., Liu, X. Q., Chen, X. M., Li, H. M. and Ding, Y. B. (2006). HAI-1 expression in villous tissue of early gestational period in women. *Sichuan Da Xue Xue Bao Yi Xue Ban* **37**, 602-605.

Fan, B., Brennan, J., Grant, D., Peale, F., Rangell, L. and Kirchhofer, D. (2007). Hepatocyte growth factor activator inhibitor-1 (HAI-1) is essential for the integrity of basement membranes in the developing placental labyrinth. *Dev. Biol.* **303**, 222-230.

Founds, S. A., Conley, Y. P., Lyons-Weiler, J. F., Jeyabalan, A., Hogge, W. A. and Conrad, K. P. (2009). Altered global gene expression in first trimester placentas of women destined to develop preeclampsia. *Placenta* **30**, 15-24.

Gao, X., Vockley, C. M., Pauli, F., Newberry, K. M., Xue, Y., Randell, S. H., Reddy, T. E. and Hogan, B. L. M. (2013). Evidence for multiple roles for grainyheadlike 2 in the establishment and maintenance of human mucociliary airway epithelium. *Proc. Natl. Acad. Sci. USA* **110**, 9356-9361.

Georgiades, P., Ferguson-Smith, A. C. and Burton, G. J. (2002). Comparative developmental anatomy of the murine and human definitive placentae. *Placenta* **23**, 3-19.

Gupta, S., Stamatoyannopoulos, J. A., Bailey, T. L. and Noble, W. S. (2007). Quantifying similarity between motifs. *Genome Biol.* **8**, R24.

Hallikas, O. K., Aaltonen, J. M., von Koskull, H., Lindberg, L.-A., Valmu, L., Kalkkinen, N., Wahlström, T., Kataoka, H., Andersson, L., Lindholm, D. et al. (2006). Identification of antibodies against HAI-1 and integrin alpha6beta4 as immunohistochemical markers of human villous cytotrophoblast. *J. Histochem. Cytochem.* **54**, 745-752.

Han, Y., Mu, Y., Li, X., Xu, P., Tong, J., Liu, Z., Ma, T., Zeng, G., Yang, S., Du, J. et al. (2011). Grhl2 deficiency impairs otic development and hearing ability in a zebrafish model of the progressive dominant hearing loss DFNA28. *Hum. Mol. Genet.* **20**, 3213-3226.

Hayashi, S., Lewis, P., Pevny, L. and McMahon, A. P. (2002). Efficient gene modulation in mouse epiblast using a Sox2Cre transgenic mouse strain. *Mech. Dev.* **119** Suppl. 1, S97-S101.

Heinz, S., Benner, C., Spann, N., Bertolino, E., Lin, Y. C., Laslo, P., Cheng, J. X., Murre, C., Singh, H. and Glass, C. K. (2010). Simple combinations of lineage-determining transcription factors prime cis-regulatory elements required for macrophage and B cell identities. *Mol. Cell* **38**, 576-589.

Huuskonen, P., Storvik, M., Reinisalo, M., Honkakoski, P., Rysä, J., Hakkola, J. and Pasanen, M. (2008). Microarray analysis of the global alterations in the gene expression in the placentas from cigarette-smoking mothers. *Clin. Pharmacol. Ther.* **83**, 542-550.

Jackman, S. M., Kong, X. and Fant, M. E. (2012). Plac1 (placenta-specific 1) is essential for normal placental and embryonic development. *Mol. Reprod. Dev.* **79**, 564-572.

Kataoka, H., Meng, J. Y., Itoh, H., Hamasuna, R., Shimomura, T., Suganuma, T. and Koono, M. (2000). Localization of hepatocyte growth factor activator inhibitor type 1 in Langhans' cells of human placenta. *Histochem. Cell Biol.* **114**, 469-475.

Kawaguchi, M., Takeda, N., Hoshiko, S., Yorita, K., Baba, T., Sawaguchi, A., Nezu, Y., Yoshikawa, T., Fukushima, T. and Kataoka, H. (2011). Membrane-bound serine protease inhibitor HAI-1 is required for maintenance of intestinal epithelial integrity. *Am. J. Pathol.* **179**, 1815-1826.

Development (2015) 142, 1125-1136 doi:10.1242/dev.113829

Klein, G., Langegger, M., Timpl, R. and Ekblom, P. (1988). Role of laminin A chain in the development of epithelial cell polarity. *Cell* **55**, 331-341.

Li, Z., Van Calcar, S., Qu, C., Cavenee, W. K., Zhang, M. Q. and Ren, B. (2003). A global transcriptional regulatory role for c-Myc in Burkitt's lymphoma cells. *Proc. Natl. Acad. Sci. USA* **100**, 8164-8169.

Lin, C.-Y., Anders, J., Johnson, M. and Dickson, R. B. (1999). Purification and characterization of a complex containing matriptase and a Kunitz-type serine protease inhibitor from human milk. *J. Biol. Chem.* **274**, 18237-18242.

Mace, K. A., Pearson, J. C. and McGinnis, W. (2005). An epidermal barrier wound repair pathway in Drosophila is mediated by grainy head. *Science* **308**, 381-385.

Mikheev, A. M., Nabekura, T., Kaddoumi, A., Bammler, T. K., Govindarajan, R., Hebert, M. F. and Unadkat, J. D. (2008). Profiling gene expression in human placentae of different gestational ages: an OPRU Network and UW SCOR Study. *Reprod. Sci.* **15**, 866-877.

Millar, I. D., Taylor, H. C., Cooper, G. J., Kibble, J. D., Barhanin, J. and Robson, L. (2006). Adaptive downregulation of a quinidine-sensitive cation conductance in renal principal cells of TWIK-1 knockout mice. *Pflugers Arch.* **453**, 107-116.

Narasimha, M., Uv, A., Krejci, A., Brown, N. H. and Bray, S. J. (2008). Grainy head promotes expression of septate junction proteins and influences epithelial morphogenesis. *J. Cell Sci.* **121**, 747-752.

Oberst, M. D., Chen, L.-Y. L., Kiyomiya, K.-I., Williams, C. A., Lee, M.-S., Johnson, M. D., Dickson, R. B. and Lin, C.-Y. (2005). HAI-1 regulates activation and expression of matriptase, a membrane-bound serine protease. *Am. J. Physiol. Cell Physiol.* **289**, C462-C470.

Pöschl, E., Schlötzer-Schrehardt, U., Brachvogel, B., Saito, K., Ninomiya, Y. and Mayer, U. (2004). Collagen IV is essential for basement membrane stability but dispensable for initiation of its assembly during early development. *Development* **131**, 1619-1628.

Pyrgaki, C., Liu, A. and Niswander, L. (2011). Grainyhead-like 2 regulates neural tube closure and adhesion molecule expression during neural fold fusion. *Dev. Biol.* **353**, 38-49.

Raffel, G. D., Chu, G. C., Jesneck, J. L., Cullen, D. E., Bronson, R. T., Bernard, O. A. and Gilliland, D. G. (2009). Ott1 (Rbm15) is essential for placental vascular branching morphogenesis and embryonic development of the heart and spleen. *Mol. Cell. Biol.* **29**, 333-341.

Rifat, Y., Parekh, V., Wilanowski, T., Hislop, N. R., Auden, A., Ting, S. B., Cunningham, J. M. and Jane, S. M. (2010). Regional neural tube closure defined by the Grainy head-like transcription factors. *Dev. Biol.* **345**, 237-245.

Schmidt, D., Wilson, M. D., Spyrou, C., Brown, G. D., Hadfield, J. and Odom, D. T. (2009). ChIP-seq: using high-throughput sequencing to discover protein-DNA interactions. *Methods* **48**, 240-248.

Schorle, H., Meier, P., Buchert, M., Jaenisch, R. and Mitchell, P. J. (1996). Transcription factor AP-2 essential for cranial closure and craniofacial development. *Nature* **381**, 235-238.

Senga, K., Mostov, K. E., Mitaka, T., Miyajima, A. and Tanimizu, N. (2012). Grainyhead-like 2 regulates epithelial morphogenesis by establishing functional tight junctions through the organization of a molecular network among claudin3, claudin4, and Rab25. *Mol. Biol. Cell* **23**, 2845-2855.

Shimomura, T., Denda, K., Kitamura, A., Kawaguchi, T., Kito, M., Kondo, J., Kagaya, S., Qin, L., Takata, H., Miyazawa, K. et al. (1997). Hepatocyte growth factor activator inhibitor, a novel Kunitz-type serine protease inhibitor. *J. Biol. Chem.* **272**, 6370-6376.

Simmons, D. G., Natale, D. R. C., Begay, V., Hughes, M., Leutz, A. and Cross, J. C. (2008). Early patterning of the chorion leads to the trilaminar trophoblast cell structure in the placental labyrinth. *Development* **135**, 2083-2091.

Sorokin, L., Sonnenberg, A., Aumailley, M., Timpl, R. and Ekblom, P. (1990). Recognition of the laminin E8 cell-binding site by an integrin possessing the alpha 6 subunit is essential for epithelial polarization in developing kidney tubules. *J. Cell Biol.* **111**, 1265-1273.

Stemmler, M. P. and Bedzhov, I. (2010). A Cdh1HA knock-in allele rescues the Cdh1-/- phenotype but shows essential Cdh1 function during placentation. *Dev. Dyn.* **239**, 2330-2344.

Stemmler, M. P., Hecht, A. and Kemler, R. (2005). E-cadherin intron 2 contains cis-regulatory elements essential for gene expression. *Development* **132**, 965-976.

Szabo, R., Molinolo, A., List, K. and Bugge, T. H. (2007). Matriptase inhibition by hepatocyte growth factor activator inhibitor-1 is essential for placental development. *Oncogene* **26**, 1546-1556.

Szabo, R., Uzzun Sales, K., Kosa, P., Shylo, N. A., Godiksen, S., Hansen, K. K., Friis, S., Gutkind, J. S., Vogel, L. K., Hummler, E. et al. (2012). Reduced prostasin (CAP1/PRSS8) activity eliminates HAI-1 and HAI-2 deficiency-associated developmental defects by preventing matriptase activation. *PLoS Genet.* **8**, e1002937.

Takahashi, Y., Carpino, N., Cross, J. C., Torres, M., Parganas, E. and Ihle, J. N. (2003). SOCS3: an essential regulator of LIF receptor signaling in trophoblast giant cell differentiation. *EMBO J.* **22**, 372-384.

Tanaka, H., Nagaike, K., Takeda, N., Itoh, H., Kohama, K., Fukushima, T., Miyata, S., Uchiyama, S., Uchinokura, S., Shimomura, T. et al. (2005). Hepatocyte growth factor activator inhibitor type 1 (HAI-1) is required for branching morphogenesis in the chorioallantoic placenta. *Mol. Cell. Biol.* **25**, 5687-5698.

Tang, T., Li, L., Tang, J., Li, Y., Lin, W. Y., Martin, F., Grant, D., Solloway, M., Parker, L., Ye, W. et al. (2010). A mouse knockout library for secreted and transmembrane proteins. *Nat. Biotechnol.* **28**, 749-755.

Tao, J., Kuliyev, E., Wang, X., Li, X., Wilanowski, T., Jane, S. M., Mead, P. E. and Cunningham, J. M. (2005). BMP4-dependent expression of Xenopus Grainyhead-like 1 is essential for epidermal differentiation. *Development* **132**, 1021-1034.

Tarabay, Y., Kieffer, E., Teletin, M., Celebi, C., Van Montfoort, A., Zamudio, N., Achour, M., El Ramy, R., Gazdag, E., Tropel, P. et al. (2013). The mammalian-specific Tex19.1 gene plays an essential role in spermatogenesis and placenta-supported development. *Hum. Reprod.* **28**, 2201-2214.

Uhlen, M., Oksvold, P., Fagerberg, L., Lundberg, E., Jonasson, K., Forsberg, M., Zwahlen, M., Kampf, C., Wester, K., Hober, S. et al. (2010). Towards a knowledge-based Human Protein Atlas. *Nat. Biotechnol.* **28**, 1248-1250.

Valouev, A., Johnson, D. S., Sundquist, A., Medina, C., Anton, E., Batzoglou, S., Myers, R. M. and Sidow, A. (2008). Genome-wide analysis of transcription factor binding sites based on ChIP-Seq data. *Nat. Methods* **5**, 829-834.

Varma, S., Cao, Y., Tagne, J.-B., Lakshminarayanan, M., Li, J., Friedman, T. B., Morell, R. J., Warburton, D., Kotton, D. N. and Ramirez, M. I. (2012). The transcription factors Grainyhead-like 2 and NK2-homeobox 1 form a regulatory loop that coordinates lung epithelial cell morphogenesis and differentiation. *J. Biol. Chem.* **287**, 37282-37295.

Werth, M., Walentin, K., Aue, A., Schönheit, J., Wuebken, A., Pode-Shakked, N., Vilianovitch, L., Erdmann, B., Dekel, B., Bader, M. et al. (2010). The transcription factor grainyhead-like 2 regulates the molecular composition of the epithelial apical junctional complex. *Development* **137**, 3835-3845.

Wilanowski, T., Tuckfield, A., Cerruti, L., O'Connell, S., Saint, R., Parekh, V., Tao, J., Cunningham, J. M. and Jane, S. M. (2002). A highly conserved novel family of mammalian developmental transcription factors related to Drosophila grainyhead. *Mech. Dev.* **114**, 37-50.

Wilanowski, T., Caddy, J., Ting, S. B., Hislop, N. R., Cerruti, L., Auden, A., Zhao, L.-L., Asquith, S., Ellis, S., Sinclair, R. et al. (2008). Perturbed desmosomal cadherin expression in grainy head-like 1-null mice. *EMBO J.* **27**, 886-897.

Yamauchi, M., Kataoka, H., Itoh, H., Seguchi, T., Hasui, Y. and Osada, Y. (2004). Hepatocyte growth factor activator inhibitor types 1 and 2 are expressed by tubular epithelium in kidney and down-regulated in renal cell carcinoma. *J. Urol.* **171**, 890-896.

Yu, Z., Lin, K. K., Bhandari, A., Spencer, J. A., Xu, X., Wang, N., Lu, Z., Gill, G. N., Roop, D. R., Wertz, P. et al. (2006). The Grainyhead-like epithelial transactivator Get-1/Grhl3 regulates epidermal terminal differentiation and interacts functionally with LMO4. *Dev. Biol.* **299**, 122-136.

Yu, Z., Mannik, J., Soto, A., Lin, K. K. and Andersen, B. (2009). The epidermal differentiation-associated Grainyhead gene Get1/Grhl3 also regulates urothelial differentiation. *EMBO J.* **28**, 1890-1903.

Zhang, J., Hagopian-Donaldson, S., Serbedzija, G., Elsemore, J., Plehn-Dujowich, D., McMahon, A. P., Flavell, R. A. and Williams, T. (1996). Neural tube, skeletal and body wall defects in mice lacking transcription factor AP-2. *Nature* **381**, 238-241.

Zhang, Y., Liu, T., Meyer, C. A., Eeckhoute, J., Johnson, D. S., Bernstein, B. E., Nusbaum, C., Myers, R. M., Brown, M., Li, W. et al. (2008). Model-based analysis of ChIP-Seq (MACS). *Genome Biol.* **9**, R137.

Supplementary Figures

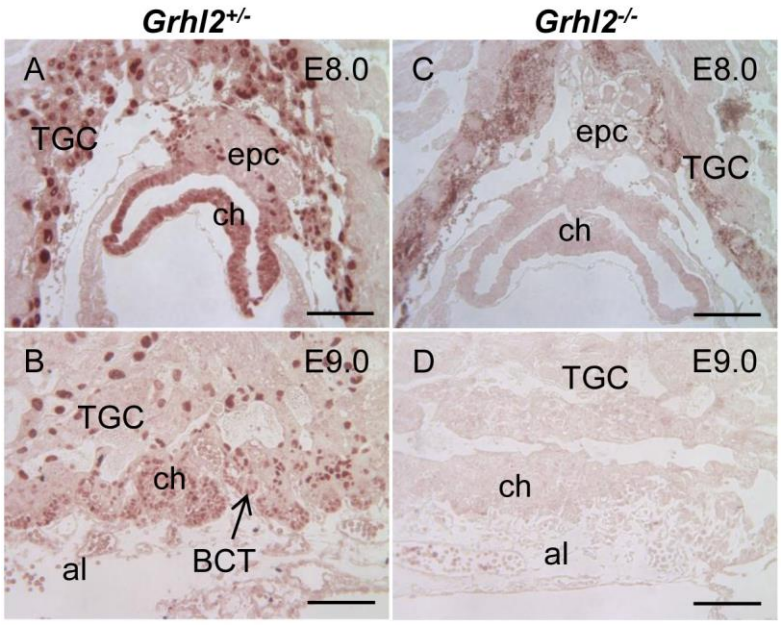

Fig. S1. GRHL2 expression pattern in the mouse placenta. GRHL2 expression analysis in control *Grhl2*$^{+/-}$ placentas at E8.0 (A) and E9.0 (B) showed that GRHL2 was highly expressed in the primary and secondary trophoblast giant cells (TGC). Moreover, GRHL2 expression was detected in the chorion (ch) at E8.0 and became restricted to the BCT cells at E9.0 (B, arrow). In contrast, no GRHL2 staining was observed in *Grhl2*$^{-/-}$ placentas at E8.0 (C) and E9.0 (D). al, allantois; epc, ectoplacental cone. Scale bar: 100 µm. Related to Fig. 1.

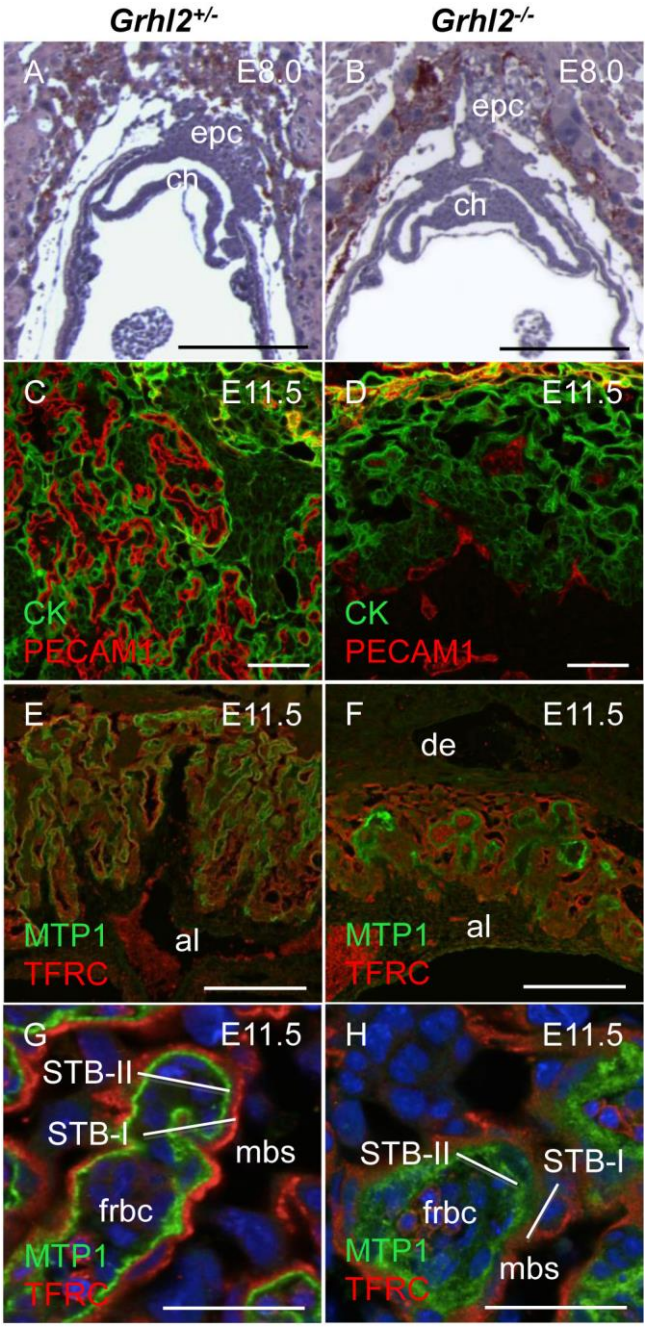

Fig. S2. Defective vascularization and trophoblast branching in *Grhl2*$^{-/-}$ placentas. (A,B) Comparison of H&E-stained sections of control *Grhl2*$^{+/-}$ and mutant placentas showed a normal placenta development of *Grhl2*$^{-/-}$ embryos until E8.0. Scale bar: 250 µm. (C,D) Immunofluorescence staining of pan-cytokeratin (CK, green) and PECAM1 (red) at E11.5 revealed that *Grhl2*$^{-/-}$ placentas exhibited remarkably fewer fetal blood vessels in the labyrinth and a compact labyrinth structure compared to controls. Scale bar: 75 µm. (E-H) Labeling of the syncytiotrophoblast (STB) layers at E11.5 by transferrin receptor (TFRC, red, STB layer I (STB-I)) and ferroportin (MTP1, green, STB layer II (STB-II)) staining (E11.5 low magnification: E, F, scale bar: 250 µm; high magnification: G, H, scale bar: 50 µm) demonstrated that trophoblast branching was initiated in *Grhl2*$^{-/-}$ placentas, but that progression of labyrinth formation was disturbed, resulting in few and simple trophoblast branches (F) compared to the complex STB network in controls (E). Higher magnification revealed an increased thickness of STB-II in mutants indicated by a broadened staining of MTP1 (H) when compared to controls (G). al, allantois; ch, chorion; de, epc, ectoplacental cone; decidua; frbc, fetal red blood cells; mbs, maternal blood sinus. Related to Fig. 2.

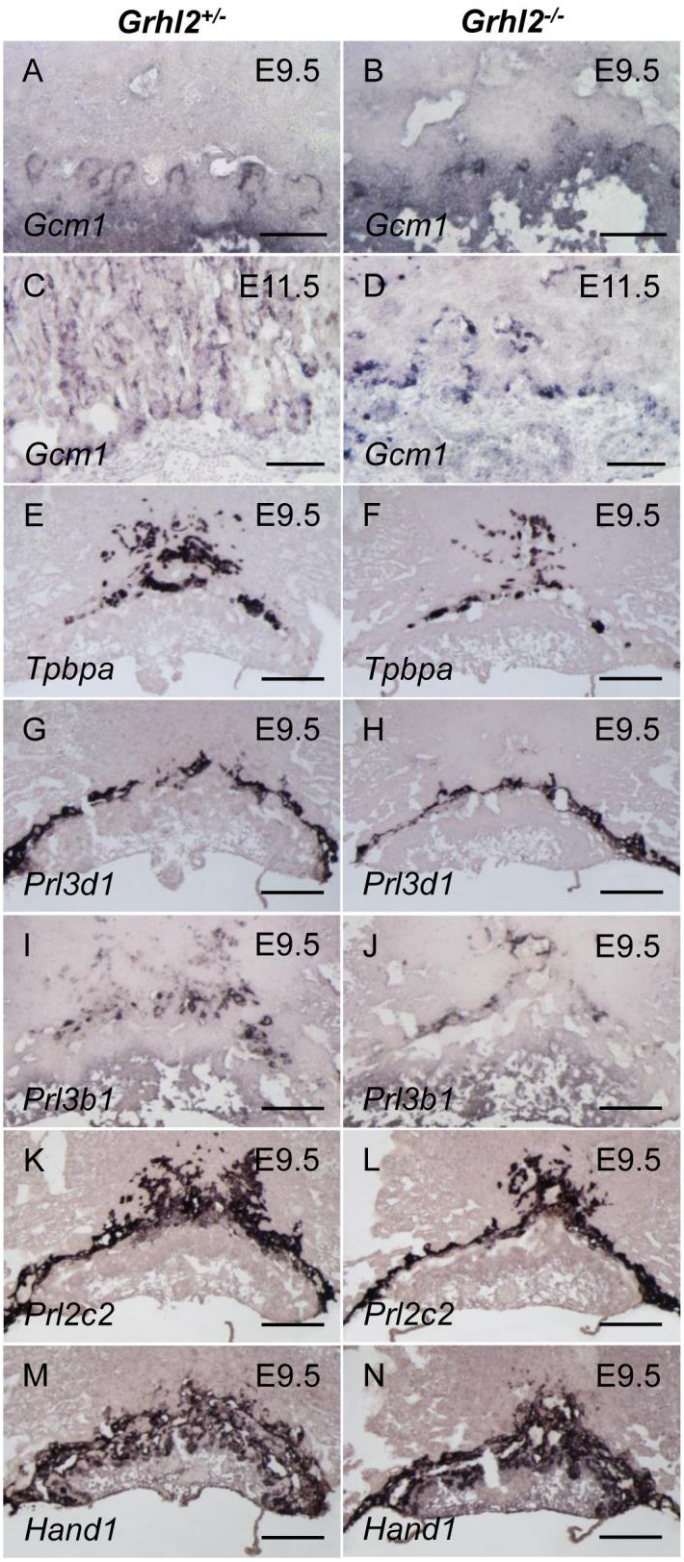

Fig. S3. Spongiotrophoblast, TGC and initiation marker for labyrinthal morphogenesis were maintained in *Grhl2*$^{-/-}$ placentas. (A-D) Branch point labeling in the chorionic trophoblast layer by *Gcm1 in situ* hybridization (ISH) showed that *Gcm1* expression was present at the sites of branch point initiation in *Grhl2*$^{-/-}$ placentas at E9.5, but the amount of *Gcm1*-positive branching initiation sites was markedly reduced (B) compared to controls (A). *Gcm1* staining at E11.5 (C,D) detecting branch points in the labyrinth revealed a massively disturbed branching morphogenesis in *Grhl2*$^{-/-}$ placentas (D). Scale bar: 100 µm. (E,F) Staining of the spongiotrophoblast marker *Tpbpa* by ISH revealed that *Tpbpa* was present in *Grhl2*$^{-/-}$ placentas at E9.5. (G-N) Giant cell markers *Prl3d1* (G,H), *Prl3b1* (I,J), *Prl2c2* (K,L) and *Hand1* (M,N) showed no substantial expression difference at E9.5. Scale bars of E9.5 placentas: 250 µm. Related to Fig. 2.

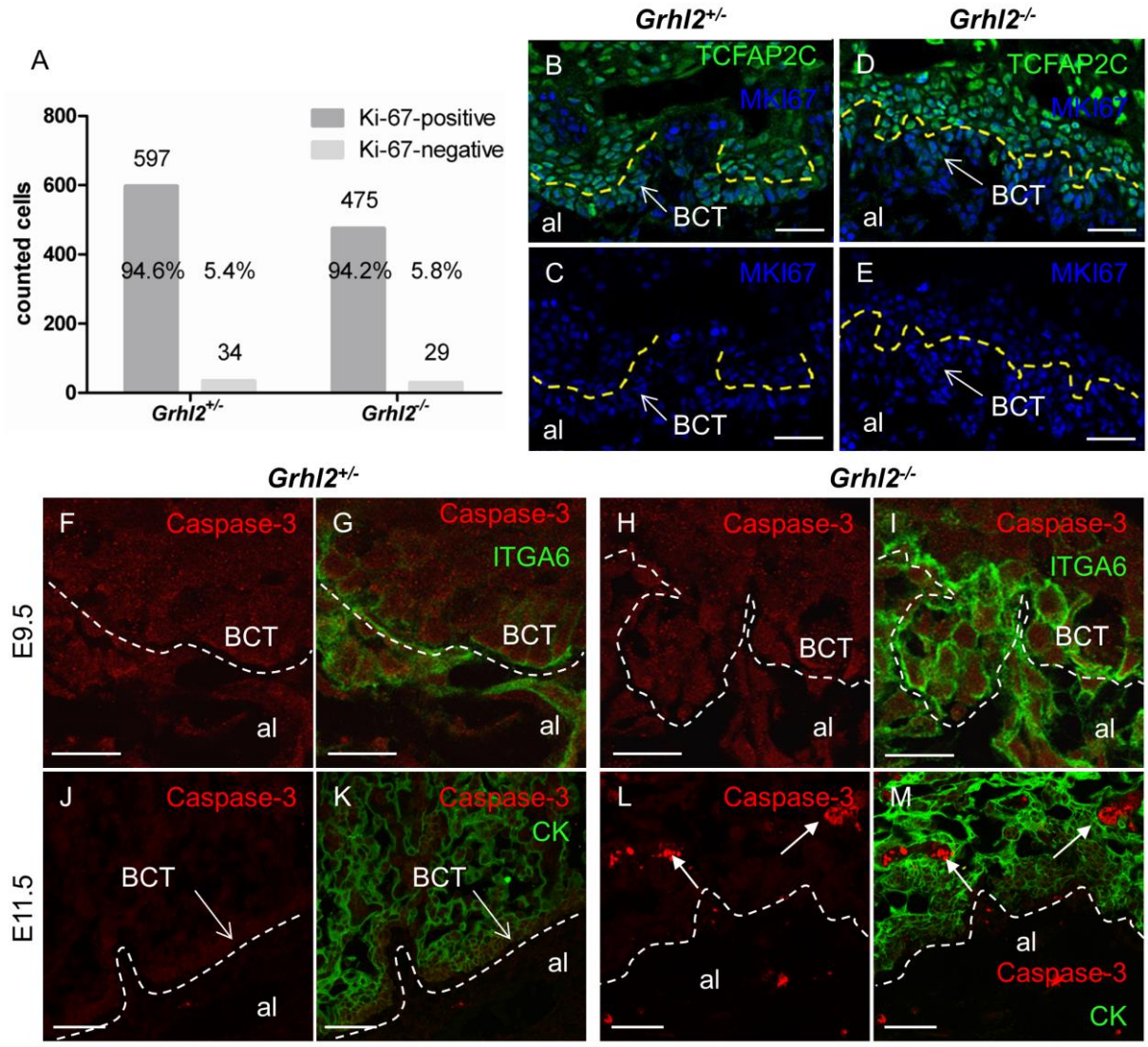

Fig. S4. Analysis of cell proliferation and apoptosis in control and *Grhl2*$^{-/-}$ placentas. (A-E) Analysis of cell proliferation via Ki-67 immunofluorescence staining showed no proliferation differences of the basal chorionic trophoblast (BCT) cells in controls and *Grhl2* mutants at E9.5 (96.6% in *Grhl2*$^{+/-}$ versus 96.4% in *Grhl2*$^{-/-}$ placentas). The yellow dashed line separates the BCT cells from overlying trophoblast cell layers. Scale bar: 100 µm. (F-M) Cell apoptosis was analyzed by active caspase-3 immunostaining (red). Co-staining with the epithelial basolateral marker integrin alpha 6 (ITGA6, green, E9.5, G,I) or with pan-cytokeratin (CK, green, E11.5, K,M) facilitated the identification of BCT cells. We found no evidence for trophoblast apoptosis in control (F,G) and *Grhl2*$^{-/-}$ placentas (H,I) at E9.5. At E11.5, several fetal blood cells were apoptotic in *Grhl2*$^{-/-}$ placentas (L,M, arrows) likely due to secondary effects originating from defective feto-maternal exchange. The white dashed lines mark the border between epithelial trophoblasts and allantois (al). Scale bar E9.5: 100 µm. Scale bar E11.5: 250 µm. Related to Fig. 2.

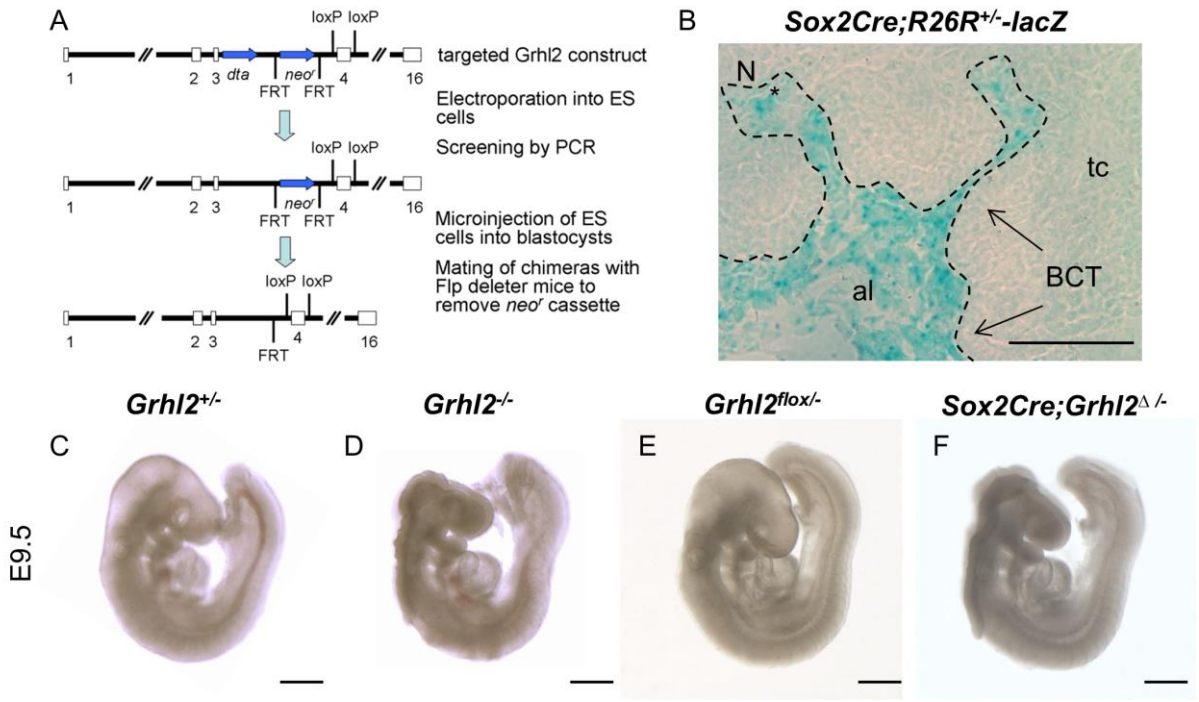

Fig. S5. Selective inactivation of *Grhl2* in epiblast-derived tissues. (A) Targeting strategy for generating a conditional *Grhl2* allele. The targeted *Grhl2* construct is depicted on top. Open boxes represent exons. The diphtheria toxin A (*dta*) and neomycin resistance (*neo*') sequences are indicated by blue arrows. *Neo*^{r} was flanked by two FRT sites, exon 4 of *Grhl2* by two loxP sites. Depicted in the middle is the targeted *Grhl2* allele after electroporation and insertion into the genome of ES cells by homologous recombination. Random integration was reduced through the presence of the *dta* cassette at the 5' end of the construct. Identification of ES cells carrying the targeted *Grhl2* allele was achieved by G418 selection and subsequent PCR. The bottom diagram represents the final floxed *Grhl2* allele after crossing of chimeric mice with Flp deleter mice to remove *neo*^{r} sequences. (B) *Sox2Cre*-mediated activation of β-galactosidase in *R26R* mice. Female *R26R* mice were bred with male *Sox2Cre* mice, and placentas of E9.5 pups were analyzed via X-gal histochemical staining. At E9.5 allantoic mesenchymal cells derived from the epiblast appeared in blue color, including fetal blood vessels (asterisks) arising from the allantois (al). In contrast, all trophectoderm-derived cell types including the basal chorionic trophoblast (BCT) cells remained unstained, indicating that *Sox2Cre*-mediated recombination occurred specifically in the epiblast-derived tissues. The dashed line marks the boundary between trophoblast compartment and allantois. tc, trophoblast cell(s). Scale bar: 100 µm. (C-F) Images of E9.5 littermate control embryos (C: *Grhl2*$^{+/-}$; E: *Grhl2*$^{flox/-}$), *Grhl2*$^{-/-}$ embryos (D) and *Sox2Cre;Grhl2*$^{\Delta/-}$ embryos (F). *Grhl2*$^{-/-}$ and *Sox2Cre;Grhl2*$^{\Delta/-}$ embryos exhibited an identical phenotype including split-face malformations, exencephaly plus anterior and lumbosacral spina bifida. Scale bar: 500 µm. Related to Fig. 3.

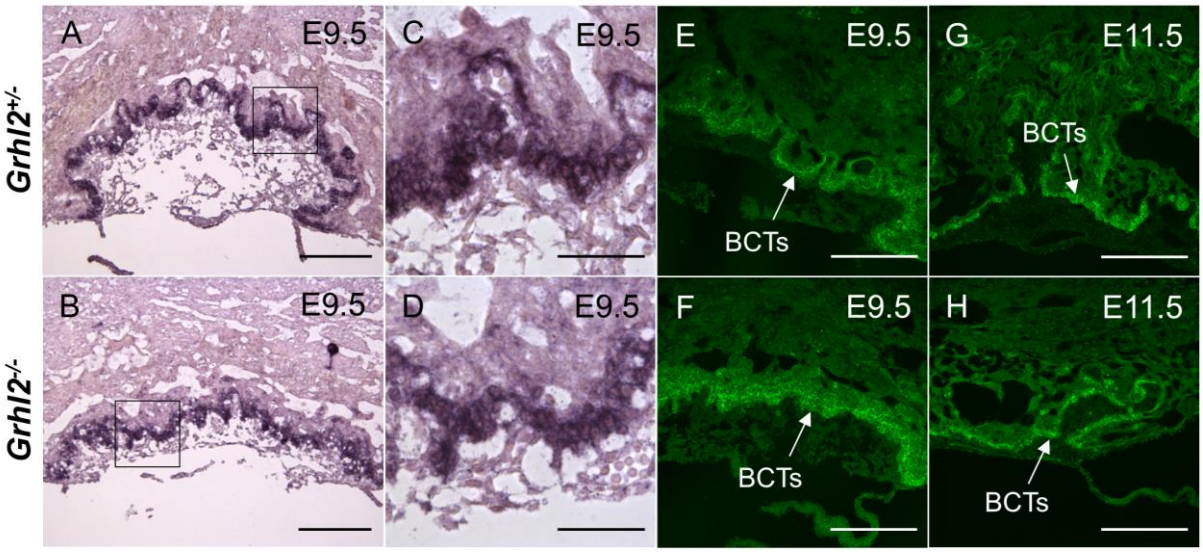

Fig. S6. *Cldn4* expression in the BCT cells of *Grhl2*$^{-/-}$ placentas is unchanged on RNA and protein level. (A-D) *In situ* hybridization on E9.5 placenta sections showed the same expression intensity for *Cldn4* in BCT cells of *Grhl2* mutant (B,D) and control placentas (A,C). Boxed regions in A,B are magnified in C,D. Scale bars A,B: 250 µm. Scale bars C,D: 75 µm. (E-H) Immunofluorescence staining revealed strong expression of CLDN4 in the BCT cells in control *Grhl2*$^{+/-}$ (E,G) as wells as in *Grhl2*$^{-/-}$ placentas (F,H) compared to overlying trophoblast cell layers, respectively. CLDN4 expression levels in BCT cells of *Grhl2*$^{-/-}$ placentas are comparable to that of controls at E9.5 (E,F) as well as E11.5 (G,H). Scale bars: 250 µm. Related to Fig. 6.

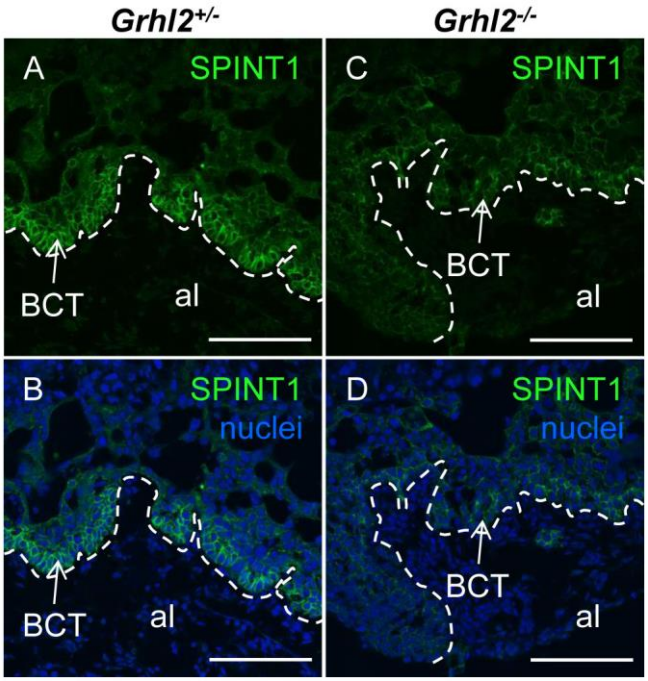

Fig. S7. GRHL2 regulated SPINT1 expression in the BCT cells of murine placentas and was necessary for normal arrangement of trophoblast epithelia. *Grhl2* ablation in murine placentas resulted in a strong downregulation of SPINT1 specifically in the BCT cells (C,D) when compared to controls (A,B) at E9.5. The weak expression of SPINT1 in the overlying trophoblast cells was maintained (C,D). Scale bar: 250 µm. Related to Fig. 6.

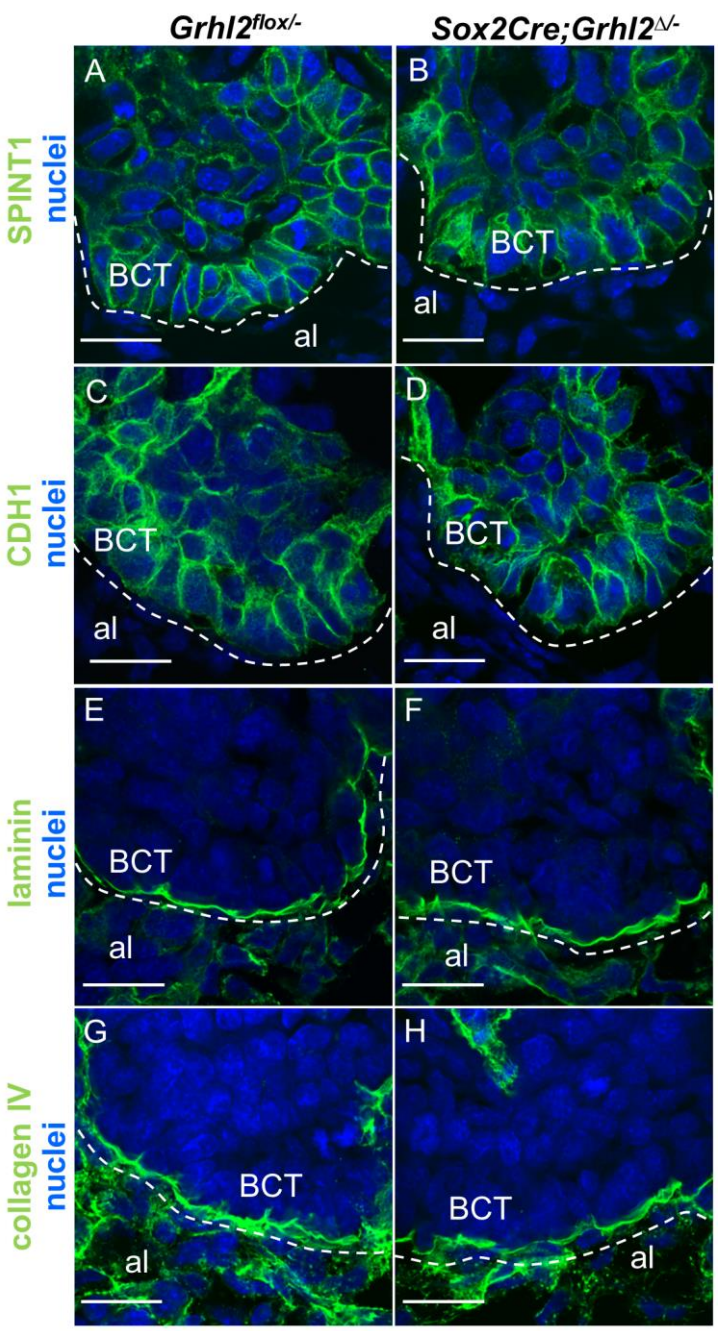

Fig. S8. Epiblast-specific deletion of *Grhl2* using *Sox2Cre* does not induce alterations in SPINT1 and CDH1 expression in BCT cells and preserves continuous basement membranes at the chorioallantoic interface. SPINT1 expression levels (A, B), CDH1 expression levels (C, D) as well as laminin (E,F) and collagen IV deposition (G, H) in BCT cells at the chorioallantoic interface (dashed lines) of *Sox2Cre;Grhl2*$^{\Delta/-}$ embryos (B,D,F,H) are identical to that of their control *Grhl2*$^{flox/-}$ littermates (A,C,E,G). Scale bar: 25 μm. al, allantois. Related to Fig. 3.

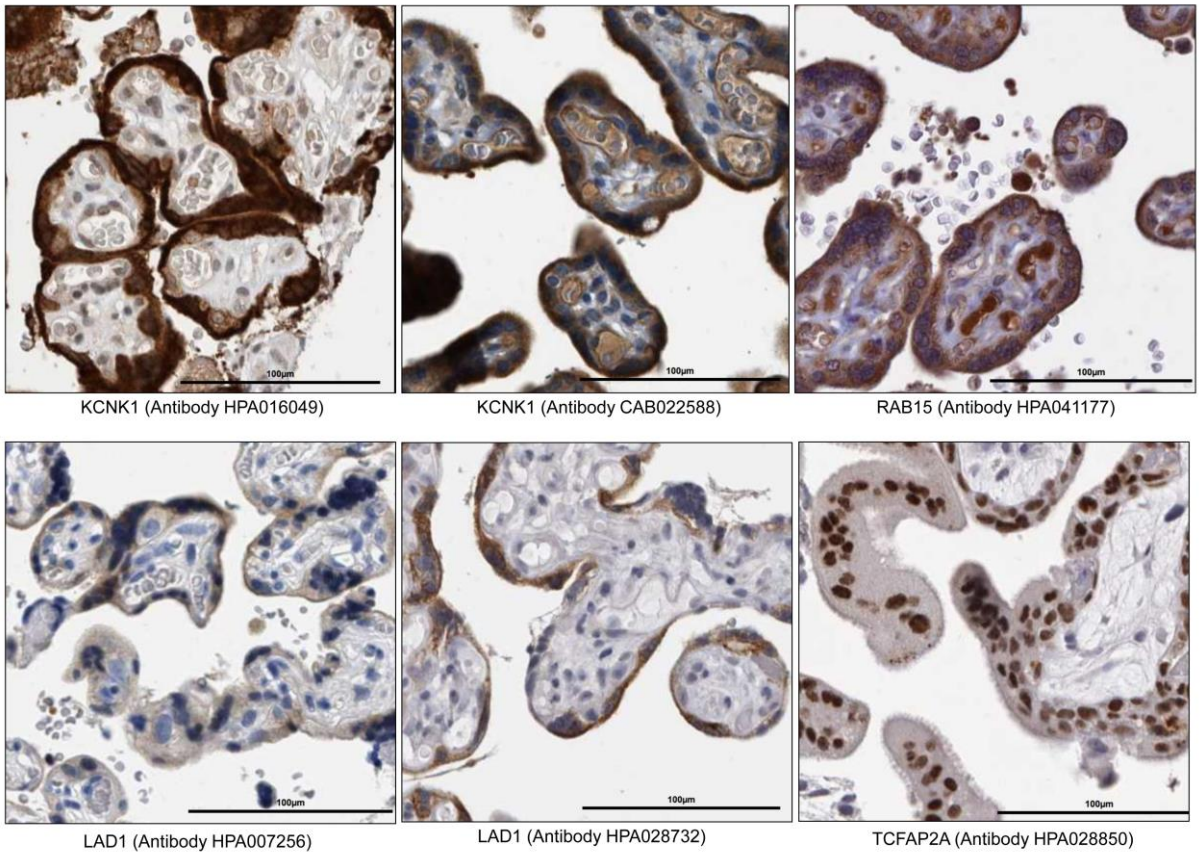

Fig. S9. Placental expression of proteins encoded by human orthologs of the *Grhl2* target gene set. Expression of the indicated proteins was identified in placenta sections from the Human Protein Database (Uhlen et al., 2010) (http://www.proteinatlas.org/). Protein name and antibody identifier (according to the Human Protein Atlas) are shown below each image. Note that all proteins are expressed in villous cytotrophoblasts and/or adjacent syncytiotrophoblasts in a domain similar to the GRHL2 expression domain. Scale bar: 100 µm. Related to Fig. 7.

Supplementary Tables

Table S1. *Grhl2* is crucial for embryonic survival in mice. Time course of lethality in mice resulting from intercrosses of *Grhl2*$^{+/lacZ4}$ and *Grhl2*$^{+/lacZ1}$ mice. Up to E11.5 the distribution of genotypes showed approximately Mendelian ratios (*Grhl2*^{lacZ4}: 20 % +/+, 54 % +/-, 26 % -/-; *Grhl2*^{lacZ1}: 27 % +/+, 44 % +/-, 29 % -/-). No *Grhl2*$^{-/-}$ embryos were found after E11.5 in the offspring of *Grhl2*^{lacZ4} and *Grhl2*^{lacZ1} intercrosses. E, embryonic day; P, postnatal day. Related to Fig. 2.

Strain	Stage	Number of mice (litter)	*Grhl2*$^{+/+}$	*Grhl2*$^{+/-}$	*Grhl2*$^{-/-}$
Grhl2$^{+/lacZ4}$ x *Grhl2*$^{+/lacZ4}$	E7.5	14 (2)	3	7	4
	E8.5	31 (3)	6	16	9
	E9.5	113 (12)	22	63	28
	E10.5	14 (2)	3	8	3*
	E11.5	16 (2)	4	7	5†
	E14.5	5 (1)	0	5	0
	P21	68	23	45	0
Grhl2$^{+/lacZ1}$ x *Grhl2*$^{+/lacZ1}$	E8.5	20 (2)	5	8	7
	E9.5	39 (5)	12	17	10
	E10.5	7 (1)	1	4	2*
	E18.5	8 (1)	4	4	0
	P21	51	19	32	0

*embryos developmentally retarded, †embryos dead

Table S2. Genes downregulated in *Grhl2*$^{-/-}$ (KO) versus control placentas (WT) at both E7.5 and E9.5 identified by microarray analysis. The top 150 genes for each time-point were considered. Fold rank indicated as WT/KO, *P*-values of log2 transformation < 0.05, gene symbols according to Illumina resource file apart from GRHL2 core target gene set. Genes in bold type display genomic GRHL2 association based on at least one GRHL2 binding peak in placental extracts (gene body ± 2 kb). Related to Fig. 4.

		E7.5				E9.5			
Probe ID	Gene name	Average WT	Average KO	Fold change (WT/KO)	Log2 *P*	Average WT	Average KO	Fold change (WT/KO)	Log2 *P*
ILMN_1246392	***Prom2***	**224.6**	**71.1**	**3.2**	**0.0010**	**1055.5**	**96.0**	**11.0**	**0.0047**
ILMN_2919393	***Tmem54***	**154.1**	**76.8**	**2.0**	**0.0040**	**500.2**	**106.0**	**4.7**	**0.0002**
ILMN_2846026	*Rhox4d*	113.8	79.5	1.4	0.0339	1108.2	308.1	3.6	0.0024
ILMN_1227260	***Lad1***	**114.0**	**74.5**	**1.5**	**0.0050**	**546.0**	**200.4**	**2.7**	**0.0068**
ILMN_1257070	*Grhl2*	127.5	74.3	1.7	0.0254	281.5	104.2	2.7	0.0128
ILMN_1259206	*Hrc*	111.8	86.1	1.3	0.0287	703.2	271.5	2.6	0.0051
ILMN_1243939	*9530027K23Rik*	109.0	82.7	1.3	0.0130	818.7	325.1	2.5	0.0017
ILMN_1260582	*LOC280487*	314.8	251.0	1.3	0.0175	2221.9	906.9	2.4	0.0225
ILMN_1217009	***Rab15***	**924.2**	**499.0**	**1.9**	**0.0003**	**4546.8**	**1888.4**	**2.4**	**0.0246**
ILMN_2502226	*Utf1*	159.1	92.4	1.7	0.0032	558.7	236.2	2.4	0.0179
ILMN_2717099	*Irx2*	143.4	89.5	1.6	0.0222	334.0	157.4	2.1	0.0250
ILMN_2859192	*Trpm5*	123.6	85.9	1.4	0.0070	364.6	175.0	2.1	0.0002
ILMN_2602938	***Smpdl3b***	**284.8**	**190.2**	**1.5**	**0.0178**	**1368.1**	**704.7**	**1.9**	**0.0110**
ILMN_1251706	***1600014K23Rik***	**120.1**	**83.6**	**1.4**	**0.0012**	**3820.5**	**2060.4**	**1.9**	**0.0165**
ILMN_1226661	***Ldoc1***	**290.6**	**168.5**	**1.7**	**0.0472**	**2752.4**	**1498.3**	**1.8**	**0.0088**
ILMN_1220726	*Satb1*	637.0	439.4	1.4	0.0140	1647.9	923.8	1.8	0.0063
ILMN_2615917	***Tex19.1***	**420.6**	**208.4**	**2.0**	**0.0126**	**5046.5**	**2838.6**	**1.8**	**0.0407**
ILMN_2538597	*LOC386405*	241.0	171.7	1.4	0.0066	1027.8	579.9	1.8	0.0197
ILMN_1220650	*1600012P17Rik*	124.9	69.8	1.8	0.0184	2829.7	1614.7	1.8	0.0001
ILMN_3009501	***Kcnk1***	**180.9**	**139.1**	**1.3**	**0.0161**	**608.4**	**348.7**	**1.7**	**0.0000**
ILMN_2518197	***Tnk1***	**78.6**	**66.5**	**1.2**	**0.0303**	**273.1**	**160.9**	**1.7**	**0.0162**
ILMN_1225712	*Iap*	1944.6	1350.4	1.4	0.0263	20243.4	12036.5	1.7	0.0447
ILMN_1229393	*LOC100040016*	83.4	65.3	1.3	0.0103	132.4	79.6	1.7	0.0421
ILMN_2648169	*Sfn*	153.4	115.9	1.3	0.0317	506.7	304.9	1.7	0.0061
ILMN_2835771	***Plac1***	**2125.8**	**1149.5**	**1.8**	**0.0233**	**11872.3**	**7177.7**	**1.7**	**0.0183**
ILMN_2637094	*Pcsk6*	230.0	141.3	1.6	0.0182	2821.6	1750.1	1.6	0.0113
ILMN_2764846	***Tcfap2a***	**350.7**	**187.7**	**1.9**	**0.0042**	**371.6**	**234.5**	**1.6**	**0.0307**
ILMN_1221585	*D030026A21Rik*	165.3	134.4	1.2	0.0456	1293.4	823.3	1.6	0.0442
ILMN_2629335	*Nxf7*	455.9	269.6	1.7	0.0393	1135.5	730.7	1.6	0.0335
ILMN_2673776	*E2f2*	204.8	171.8	1.2	0.0032	406.6	263.5	1.5	0.0005
ILMN_2837779	*Trpv2*	258.7	188.6	1.4	0.0266	1791.2	1175.6	1.5	0.0271
ILMN_1237186	***Spint1***	**413.1**	**329.5**	**1.3**	**0.0092**	**2628.9**	**1733.9**	**1.5**	**0.0432**
ILMN_2588474	*Homer2*	848.9	608.8	1.4	0.0158	3343.3	2212.5	1.5	0.0299

Table S3. Top overlapping gene ontology terms (*P*<0.05) for genes displaying GRHL2 association based on placental ChIP-seq data (gene body ± 2 kb) and for the intersection of the top 150 downregulated genes in E7.5 and E9.5 *Grhl2*$^{-/-}$ versus control placentas as determined by microarray analysis. GO terms with less than four ancestor terms, less than two or more than 1000 genes in term and less than two target genes in term have been removed. Gene ontology was performed using HOMER. Related to Fig. 4.

Top overlapping ontology terms of ChIP-seq- and microarray data								
		ChIP-seq				Microarray		
Term	Name	*P*-value	Genes in term	Target genes in term	Gene names	*P*-value	Genes in term	Target genes in term
GO:0060429	epithelium development	0,0000	548	104	Shroom3,Tfap2c,Rbm15,Car2,Smad3,Spint1,Elf5,Map3k7,Esr1,Evpl,Epb4.1l5,Mesp1,Dag1,Gatad2a,Igf1r,Psen1,Kif26b,Pard3,Gpc3,Stat6,Kazn,Upk2,Map2k1,Tead2,Sema3c,Mtss1,Met,Hhip,Ift88,Tsg101,Cecr2,Ovol2,Nckap1,Psap,Zfp568,Tek,Tgm3,Trp63,Ncoa3,Prlr,Bmpr2,Egfr,Tfap2a,Numa1,Myo1e,Tgfbr3,Fras1,Tgm1,Numb,Hs2st1,Ppp3r1,Notch2,Nodal,Ctnnd1,Dlc1,Fzd7,Tmem67,Irf6,Eya1,Wnt7b,Rxra,Dlg1,Pxn,Frem2,B4galt1,Car9,Tgm2,Upk1a,Tead1,Hdac5,Lrp5,Nfib,Jak2,Jup,Trim71,Grhl2,Ryr2,Tfap2b,Phactr4,Lama1,Celsr1,Src,Kdm2b,F11r,Dsg4,Vasp,Dsp,Smad2,Pbx1,Egf,Dlg3,C2cd3,Rac1,Ctsh,Lamb2,Sema5a,Fgfr1,Hectd1,Pde4d,Mir203,Pde2a,Ski,Pml,Pou2f3	0,0052	4	Sfn,Tfap2a,Grhl2,Spint1
GO:0002009	morphogenesis of an epithelium	0,0000	372	70	Tfap2c,Shroom3,Rbm15,Car2,Smad3,Spint1,Map3k7,Esr1,Epb4.1l5,Mesp1,Dag1,Gatad2a,Igf1r,Psen1,Kif26b,Pard3,Gpc3,Tead2,Sema3c,Mtss1,Hhip,Met,Cecr2,Ovol2,Nckap1,Zfp568,Tek,Trp63,Ncoa3,Tfap2a,Egfr,Fras1,Hs2st1,Ppp3r1,Notch2,Nodal,Ctnnd1,Dlc1,Tmem67,Eya1,Wnt7b,Dlg1,Pxn,Frem2,B4galt1,Car9,Tgm2,Tead1,Hdac5,Lrp5,Jup,Trim71,Grhl2,Ryr2,Phactr4,Lama1,Celsr1,Src,Kdm2b,Vasp,Pbx1,Egf,Dlg3,C2cd3,Ctsh,Fgfr1,Sema5a,Hectd1,Ski,Pml	0,0122	3	Tfap2a,Grhl2,Spint1
GO:0048729	tissue morphogenesis	0,0001	489	84	Tfap2c,Shroom3,Rbm15,Car2,Smad3,Spint1,Pkp2,Map3k7,Esr1,Tcf7l1,Epb4.1l5,Mesp1,Twsg1,Mylk,Gatad2a,Dag1,Igf1r,Psen1,Kif26b,Pard3,Gpc3,Prkaca,Tead2,Sema3c,Mtss1,Hhip,Met,Cecr2,Ovol2,Nckap1,Smad1,Zfp568,Tek,Trp63,Ncoa3,Bmpr2,Tfap2a,Egfr,Tgfbr3,Fras1,Hs2st1,Ppp3r1,Notch2,Nodal,Ctnnd1,Dlc1,Tmem67,Eya1,Wnt7b,Rxra,Dlg1,Pxn,Frem2,B4galt1,Car9,Tgm2,Tead1,Hdac5,Lrp5,Jup,Grhl2,Trim71,Ryr2,Phactr4,Lama1,Celsr1,Src,Kdm2b,Vasp,Atp7a,Macf1,Dsp,Egf,Smad2,Pbx1,Dlg3,C2cd3,Ctsh,Fgfr1,Sema5a,Hectd1,Ski,Zfpm1,Pml	0,0251	3	Tfap2a,Grhl2,Spint1
GO:0030855	epithelial cell differentiation	0,0004	232	44	Tfap2c,Shroom3,Rxra,B4galt1,Elf5,Esr1,Upk1a,Evpl,Epb4.1l5,Mesp1,Nfib,Pard3,Kazn,Upk2,Lama1,Map2k1,F11r,Dsg4,Mtss1,Ift88,Tsg101,Dsp,Psap,Rac1,Tgm3,Trp63,Prlr,Lamb2,Bmpr2,Tfap2a,Numa1,Myo1e,Tgm1,Numb,Pde4d,Pde2a,Ppp3r1,Mir203,Ctnnd1,Fzd7,Irf6,Pou2f3,Eya1,Wnt7b	0,0364	2	Sfn,Tfap2a
GO:0043588	skin development	0,0045	58	14	Atp8a2,Ovol1,Tfap2c,Tfap2a,Atp7a,Psen1,Jup,Fras1,Pdgfa,Dsp,Tcf7l1,Irf6,Tgm3,Trp63	0,0026	2	Sfn,Tfap2a
GO:0014020	primary neural tube formation	0,0058	78	17	Tead2,Kdm2b,Shroom3,Vasp,Cecr2,Ovol2,Nckap1,Gatad2a,Tfap2a,Trim71,Grhl2,Hectd1,Ski,Phactr4,Nodal,Dlc1,Celsr1	0,0046	2	Tfap2a,Grhl2
GO:0009790	embryo development	0,0088	939	130	Etl4,Tfap2c,Shroom3,Rbbp8,Elf3,Smad3,Spint1,Map3k7,Prkdc,Gata2,Tcf7l1,Hspg2,Twsg1,Tfeb,Ssbp3,Psen1,Chd7,Psmc3,Satb2,Bcr,Tenm4,Gpc3,Foxp2,Cdh23,Map2k1,Tead2,Cecr2,Ovol2,G2e3,Nckap1,Smad1,Mecp2,Col4a3bp,Trp63,E4f1,Bmpr2,Mll1,Tfap2a,Egfr,Myo1e,Foxk1,Zmiz1,Notch2,Nodal,Tdgf1,Ncor2,Eya1,Clic5,Wnt7b,Mir96,Rxra,Dlg1,Tead1,Mbd3,Jup,Tanc2,Ryr2,Hsd17b2,Chst11,Foxp1,Ppap2b,Vasp,Nipbl,Inpp5b,Smad2,Pbx1,Rac1,Psmc4,Fgfr1,Lmbr1,Gtf2ird1,Tjp1,Plac1,Gab1,Keap1,Efna1,Mesp1,Epb4.1l5,Abcg2,Gatad2a,Abi1,Apba1,Rictor,Ppp1r13l,Mkl2,Tet3,Prkaca,Hoxd3,Ift88,Supt20,Kif16b,Rab14,Mdfi,Zfp568,Plcg1,Bcl2l1,Chrna9,Lrp4,Tgfbr3,Hdac1,Dab2,Hs2st1,Lims1,Dlc1,Fzd7,Ell,Gna12,Ankrd11,Myh9,Gnaq,Lrp5,Hopx,Trim71,Grhl2,Cubn,Zfat,Phactr4,Dnmt3a,Celsr1,Kdm2b,Pik3cb,Macf1,Runx2,Dscaml1,C2cd3,Hmx2,Kif1b,Hectd1,Ski,Zfpm1	0,0066	5	Tfap2a,Plac1,Grhl2,Pcsk6,Spint1
GO:0008544	epidermis	0,0121	195	33	Tfap2c,Fa2h,Pdgfa,Gab1,Atp2c1,Tcf7l1	0,0020	3	Satb1,Sfn,Tf

	development				,Evpl,Psen1,Jup,Mreg,Edar,Kazn,Celsr1,Map2k1,Atp8a2,Dsg4,Atp7a,Tsg101,Dsp,Tgm3,Trp63,Lrp4,Ovol1,Tfap2a,Zdhhc21,Egfr,Fras1,Tgm1,Hdac1,Tfdp1,Ctnnd1,Irf6,Pou2f3			ap2a
GO:0035148	tube formation	0,0128	118	22	Tead2,Kdm2b,Shroom3,Vasp,Cecr2,Ovol2,Nckap1,Map3k7,Tgm2,Gatad2a,Tfap2a,Grhl2,Trim71,Hectd1,Hs2st1,Dab2ip,Nodal,Ski,Phactr4,Dlc1,Edar,Celsr1	0,0103	2	Tfap2a,Grhl2
GO:0006812	cation transport	0,0133	640	91	Slc23a2,Slc22a4,Anxa6,Atp5s,Piezo1,Park2,Kcnma1,Cacna1d,Syk,Slc39a8,Slc11a1,Atp2b4,Cacnb4,Slc9b1,Calcrl,Adra1a,Psen1,Slc24a6,Atp2c2,Piezo2,Vdac1,Nfatc1,Kcnd3,Cdh23,Slc12a8,Atp8a2,Stim1,Armc1,Slc10a7,Ibtk,Uqcr11,Kcnip3,Grin2a,Plcg1,Slc40a1,Chrna9,Kcnq1,Atp8b1,Slc20a2,Camk2d,Slc10a6,Atp9a,Kcnn3,Lmtk2,Kcnj16,Cltc,Slc6a20a,Atp6v1d,Slc39a1,Atp10a,Abcc1,Kcnb2,Slc38a4,Nipa1,Atp2c1,Scnn1a,Atp1a1,Kcnj6,Cox7a2l,Dnm2,Slc39a11,Kcnk1,Slc9a2,Slc9a1,Atp6v1c2,Tcn2,Itpr1,Ryr2,Kcnh6,Sfxn5,Atp11a,Atp9b,Trpm4,Scn7a,Prkce,Slc5a1,Zdhhc17,Cacna1c,Atp7a,Tusc3,Scara5,Slc28a3,Trpc6,Cacna2d1,Cnnm2,Atp6v1g1,Slc9a3r1,Cacna1s,Kcnj15,Slc30a4,Tmem66	0,0494	3	Kcnk1,Trpv2,Trpm5
GO:0016331	morphogenesis of embryonic epithelium	0,0155	134	24	Tead2,Kdm2b,Shroom3,Vasp,Cecr2,Ovol2,Nckap1,Map3k7,Zfp568,Epb4.1l5,Trp63,Tfap2a,Gatad2a,Jup,Grhl2,Trim71,Hectd1,Hs2st1,Nodal,Phactr4,Ski,Dlc1,Celsr1,Wnt7b	0,0131	2	Tfap2a,Grhl2
GO:0030001	metal ion transport	0,0162	480	70	Slc23a2,Slc22a4,Anxa6,Kcnma1,Cacna1d,Slc39a8,Slc11a1,Atp2b4,Cacnb4,Calcrl,Adra1a,Psen1,Slc24a6,Atp2c2,Vdac1,Nfatc1,Cdh23,Kcnd3,Slc12a8,Stim1,Armc1,Slc10a7,Ibtk,Kcnip3,Grin2a,Plcg1,Slc40a1,Kcnq1,Slc20a2,Camk2d,Slc10a6,Kcnn3,Lmtk2,Kcnj16,Cltc,Slc39a1,Kcnb2,Slc38a4,Nipa1,Atp2c1,Scnn1a,Atp1a1,Kcnj6,Slc39a11,Dnm2,Kcnk1,Slc9a2,Slc9a1,Tcn2,Itpr1,Ryr2,Kcnh6,Scn7a,Trpm4,Prkce,Zdhhc17,Slc5a1,Cacna1c,Atp7a,Tusc3,Scara5,Slc28a3,Trpc6,Cacna2d1,Cnnm2,Slc9a3r1,Cacna1s,Kcnj15,Slc30a4,Tmem66	0,0239	3	Kcnk1,Trpv2,Trpm5
GO:0009913	epidermal cell differentiation	0,0165	80	16	Tfap2c,Dsg4,Fa2h,Tsg101,Dsp,Evpl,Tgm3,Trp63,Tfap2a,Tgm1,Hdac1,Ctnnd1,Irf6,Kazn,Pou2f3,Map2k1	0,0048	2	Sfn,Tfap2a
GO:0048598	embryonic morphogenesis	0,0166	504	73	Shroom3,Smad3,Spint1,Map3k7,Efna1,Gata2,Hspg2,Epb4.1l5,Mesp1,Twsg1,Gatad2a,Psen1,Chd7,Satb2,Bcr,Tenm4,Gpc3,Prkaca,Cdh23,Hoxd3,Tead2,Ift88,Kif16b,Supt20,Cecr2,Ovol2,Nckap1,Mdfi,Smad1,Zfp568,Trp63,Lrp4,Chrna9,Bmpr2,Tfap2a,Hdac1,Hs2st1,Notch2,Nodal,Tdgf1,Dlc1,Eya1,Clic5,Wnt7b,Mir96,Dlg1,Gna12,Tead1,Gnaq,Lrp5,Jup,Grhl2,Trim71,Ryr2,Chst11,Phactr4,Ppap2b,Celsr1,Kdm2b,Vasp,Nipbl,Macf1,Smad2,Pbx1,Runx2,Dscaml1,C2cd3,Rac1,Fgfr1,Hmx2,Hectd1,Lmbr1,Ski	0,0271	3	Tfap2a,Grhl2,Spint1
GO:0030216	keratinocyte differentiation	0,0167	67	14	Tfap2c,Dsg4,Tfap2a,Tgm1,Tsg101,Dsp,Ctnnd1,Kazn,Evpl,Irf6,Pou2f3,Tgm3,Map2k1,Trp63	0,0034	2	Sfn,Tfap2a
GO:0060606	tube closure	0,0177	74	15	Tead2,Kdm2b,Shroom3,Tfap2a,Vasp,Gatad2a,Grhl2,Trim71,Cecr2,Hectd1,Nckap1,Phactr4,Ski,Dlc1,Celsr1	0,0042	2	Tfap2a,Grhl2
GO:0009792	embryo development ending in birth or egg hatching	0,0191	602	85	Etl4,Tfap2c,Shroom3,Rbbp8,Elf3,Smad3,Spint1,Gab1,Map3k7,Prkdc,Keap1,Gata2,Hspg2,Abcg2,Epb4.1l5,Tfeb,Gatad2a,Abi1,Ssbp3,Psen1,Apba1,Chd7,Psmc3,Satb2,Mkl2,Map2k1,Hoxd3,Tead2,Ift88,Cecr2,Ovol2,G2e3,Nckap1,Mdfi,Zfp568,Plcg1,Bcl2l1,Col4a3bp,Tfap2a,Egfr,Myo1e,Tgfbr3,Lims1,Zmiz1,Dab2,Notch2,Nodal,Tdgf1,Dlc1,Ncor2,Eya1,Wnt7b,Ell,Rxra,Dlg1,Gna12,Ankrd11,Myh9,Mbd3,Hopx,Tanc2,Grhl2,Trim71,Hsd17b2,Cubn,Chst11,Foxp1,Phactr4,Zfat,Celsr1,Kdm2b,Vasp,Nipbl,Inpp5b,Smad2,Pbx1,Runx2,Dscaml1,C2cd3,Psmc4,Fgfr1,Hectd1,Ski,Tjp1,Plac1	0,0073	4	Tfap2a,Plac1,Grhl2,Spint1
GO:0043009	chordate embryonic development	0,0198	595	84	Etl4,Tfap2c,Shroom3,Rbbp8,Elf3,Smad3,Spint1,Gab1,Map3k7,Prkdc,Keap1,Gata2,Hspg2,Epb4.1l5,Tfeb,Gatad2a,Abi1,Ssbp3,Psen1,Apba1,Chd7,Psmc3,Satb2,Mkl2,Map2k1,Hoxd3,Tead2,Ift88,Cecr2,Ovol2,G2e3,Nckap1,Mdfi,Zfp568,Plcg1,Bcl2l1,Col4a3bp,Tfap2a,Egfr,Myo1e,Tgfbr3,Lims1,Zmiz1,Dab2,Notch2,Nodal,Tdgf1,Dlc1,Ncor2,Eya1,Wnt7b,Ell,Rxra,Dlg1,Gna12,Ankrd11,Myh9,Mbd3,Hopx,Tanc2,Grhl2,Trim71,Hsd17b2,Cubn,Chst11,Foxp1,Phactr4,Zfat,Celsr1,Kdm2b,Vasp,Nipbl,Inpp5b,Smad2,Pbx1,Runx2,Dscaml1,C2cd3,Psmc4,Fgfr1,Hectd1,Ski,Tjp1,Plac1	0,0070	4	Tfap2a,Plac1,Grhl2,Spint1
GO:0034765	regulation of ion transmembrane transport	0,0250	243	38	Kcnj16,Kcnma1,Plcb1,Cacna1d,Fgf12,Kcnb2,Homer1,Cacnb4,Kcnj6,Kcnk1,Ppargc1a,Ryr2,Trpm4,Scn7a,Reln,Vdac1,Kcnd3,Stim1,Cacna1c,Casq2,Trim27,	0,0038	3	Kcnk1,Trpv2,Trpm5

					Egf,Kcnip3,Plcg1,Clcn3,Trpc6,Dapk1,Kcnq1,Cacna2d1,Ano6,Acsl5,Slc9a3r1,Cacna1s,Kcnj15,Nedd4l,Pla2g6,Clic5,Hk1			
GO:0043269	regulation of ion transport	0,0259	444	64	Kcnma1,Plcb1,Cacna1d,Fgf12,Syk,Mgea5,Cacnb4,Mylk,Il1rn,Ppargc1a,Akt3,Il13,Stk39,Reln,Vdac1,Kcnd3,Stim1,Casq2,Trim27,Kcnip3,Plcg1,Kcnq1,Ano6,Camk2d,Nedd4l,Sptbn4,Clic5,Hk1,Kcnj16,Diap1,Dlg1,Sgk1,Kcnb2,Ptk2b,Homer1,Myh9,Atp1a1,Gnaq,Kcnj6,Chrm1,Kcnk1,Itpr1,Ryr2,Scn7a,Trpm4,Ubash3b,P2ry2,Prkce,Cacna1c,Chrm3,Egf,Rtn4,Clcn3,Dapk1,Trpc6,Cacna2d1,Acsl5,Slc9a3r1,Cacna1s,Plcb4,Kcnj15,Pml,Pla2g6,Tmem66	0,0195	3	Kcnk1,Trpv2,Trpm5
GO:0034762	regulation of transmembrane transport	0,0272	252	39	Kcnj16,Kcnma1,Plcb1,Cacna1d,Fgf12,Kcnb2,Homer1,Cacnb4,Kcnj6,Kcnk1,Ppargc1a,Ryr2,Trpm4,Scn7a,Reln,Vdac1,Kcnd3,Stim1,Cacna1c,Casq2,Trim27,Egf,Kcnip3,Plcg1,Clcn3,Lamtor1,Trpc6,Dapk1,Kcnq1,Cacna2d1,Ano6,Acsl5,Slc9a3r1,Cacna1s,Kcnj15,Nedd4l,Pla2g6,Clic5,Hk1	0,0042	3	Kcnk1,Trpv2,Trpm5
GO:0030198	extracellular matrix organization	0,0311	150	25	Col14a1,Fbln1,Fshr,Atp7a,Olfml2a,Elf3,B4galt1,Spint1,Tnr,B4galt7,Hspg2,Mpzl3,App,Lamb2,Ptk2,Dag1,Tfap2a,Myo1e,Col4a3,Csgalnact1,Col19a1,Thsd4,Rxfp1,Abi3bp,Fbln5	0,0162	2	Tfap2a,Spint1
GO:0001701	in utero embryonic development	0,0357	381	55	Ell,Tfap2c,Rxra,Rbbp8,Elf3,Gna12,Smad3,Spint1,Gab1,Ankrd11,Keap1,Gata2,Myh9,Epb4.1l5,Tfeb,Mbd3,Gatad2a,Hopx,Apba1,Chd7,Tanc2,Grhl2,Psmc3,Cubn,Hsd17b2,Mkl2,Zfat,Foxp1,Map2k1,Ift88,Inpp5b,Ovol2,G2e3,Nckap1,Smad2,Mdfi,Zfp568,Plcg1,C2cd3,Bcl2l1,Col4a3bp,Psmc4,Egfr,Fgfr1,Myo1e,Tgfbr3,Zmiz1,Dab2,Notch2,Nodal,Tdgf1,Tjp1,Plac1,Ncor2,Wnt7b	0,0130	3	Plac1,Grhl2,Spint1
GO:0001890	placenta development	0,0382	131	22	Rxra,Hsp90ab1,Met,Rbm15,Spint1,Gab1,Ovol2,Mdfi,Zfp568,Gata2,Prdx3,Tfeb,Egfr,Hsd17b2,Pbrm1,Notch2,Nodal,Birc2,Zfat,Plac1,Map2k1,Wnt7b	0,0125	2	Plac1,Spint1
GO:0001558	regulation of cell growth	0,0399	290	43	Caprin2,Wisp2,Col14a1,Hrg,Sgk1,Map2k5,Adam17,Smad3,Ptprj,Tnr,Gsk3a,Usp47,Ptk2b,Akap6,Cdh13,Rab11a,Eaf2,Ptk2,Slc9a1,Psrc1,Ppp1r9b,Dab2ip,Gas2l1,Ddx3x,Fbp1,Dscam,Osgin1,Cda,Tsg101,Mul1,Sema4d,Tnk1,Rtn4,Ncoa3,Bmpr2,Sh3bp4,Foxk1,Hspa1b,Dab2,Sertad2,Pml,Kif26a,Enpp1	0,0062	3	Sfn,Trpv2,Tnk1
GO:0072175	epithelial tube formation	0,0402	110	19	Tead2,Kdm2b,Shroom3,Vasp,Cecr2,Ovol2,Nckap1,Map3k7,Gatad2a,Tfap2a,Grhl2,Trim71,Hectd1,Hs2st1,Ski,Phactr4,Nodal,Dlc1,Celsr1	0,0090	2	Tfap2a,Grhl2
GO:0001838	embryonic epithelial tube formation	0,0402	110	19	Tead2,Kdm2b,Shroom3,Vasp,Cecr2,Ovol2,Nckap1,Map3k7,Gatad2a,Tfap2a,Grhl2,Trim71,Hectd1,Hs2st1,Ski,Phactr4,Nodal,Dlc1,Celsr1	0,0090	2	Tfap2a,Grhl2

Table S4. Primers used for the validation of *neo*^{r} excision in floxed *Grhl2* mice, genotyping of floxed *Grhl2* mice without *neo*^{r} and *Flp* deleter mice, *Sox2Cre* and *R26R-LacZ* mice. Related to Fig. 3.

	Forward primer sequence 5‘ to 3‘	Reverse primer sequence 5‘ to 3‘	PCR product length
floxed exon 4 with *neo*^{r} floxed exon 4 without *neo*^{r} wild-type exon 4	CGTGATATTGCTGAAGAGCTTG CCAGCTCTATCTCCTGAGAG CCAGCTCTATCTCCTGAGAG	TGTGTTCAGATCGGTGACAG TGTGTTCAGATCGGTGACAG TGTGTTCAGATCGGTGACAG	788 bp 683 bp 541 bp
floxed exon 4 wild-type exon 4	CCAACCTTCCCTTTCCATTC CCAACCTTCCCTTTCCATTC	AGAGGACTTGAAGGTCGGAG AGAGGACTTGAAGGTCGGAG	672 bp 564 bp
R26Fki (FLPe) allele	CCCATTCCATGCGGGGTATCG	GCATCTGGGAGATCACTGAG	700 bp
Sox2Cre allele wild-type allele	GCGGTCTGGCAGTAAAAACTATC CTAGGCCACAGAATTGAAAGATCT	GTGAAACAGCATTGCTGTCACTT GTAGGTGGAAATTCTAGCATCATCC	100 bp 324 bp
R26R-lacZ allele wild-type allele	AAAGTCGCTCTGAGTTGTTAT AAAGTCGCTCTGAGTTGTTAT	GCGAAGAGTTTGTCCTCAACC GGAGCGGGAGAAATGGATATG	314 bp 600 bp

Table S5. Primers used for screening of ES cells to generate floxed *Grhl2* mice. Related to Fig. 3.

	Forward primer sequence 5‘ to 3‘	Reverse primer sequence 5‘ to 3‘	PCR product length
Validation of homologous recombination at 5‘ end	ACAAGGAAGGTGAGGATGAG	CTAGTGAGACGTGCTACTTC	2349 bp floxed allele
Validation of homologous recombination at 3‘ end	CCAACCTTCCCTTTCCATTC	AGAGGACTTGAAGGTCGGAG	672 bp floxed allele 564 bp wild-type allele

Table S6. Riboprobes for *in situ* hybridization. Related to Fig. S3.

Target gene	Linearization for anti-sense probe	Polymerase for anti-sense probe	Insert size	Reference
Tpbpa	EcoRI	Sp6	630 bp	Francois Guillemot
Prl3d1	HindIII	Sp6	800 bp	Malgorzata Gasperowicza/ James Cross
Prl3b1	HindIII	T7	815 bp	Janet Rossant
Prl2c2	HindIII	T7	800 bp	Janet Rossant
Handl	SalI	T7	1475 bp	James Cross
Gcm1	XhoI	T7	1521 bp	Malgorzata Gasperowicza/ James Cross

Table S7. qPCR primers for expression analysis of the *Grhl2* target gene set. Related to Fig. 5.

Target gene	Forward primer sequence 5' to 3'	Reverse primer sequence 5' to 3'
Spint1	ATGTGCAAGGAATCTCACCGAA	CACAGCGTTCACTGAATGGG
Kcnk1	TCTGTGCTGGAGGATGACTG	TGATGTGAACCAGGTCTTCG
Smpdl3b	CAACACAGGTGCCCCCATAA	TGTACATTCGCCTGCCTCAG
Plac1	GTGTCCTGTGCTGCCCCTCG	GGTGGGCAGCTGCAGTTGGG
Tmem54	GGAGGAGAAGGATGGAAGCG	CAGCACCTTCCGGAACTCAT
Prom2	CCTCGTCTTCGTCACTTTCC	TCCAGGTGCTTATCCAGGTC
Ldoc1	CGCCTTTTCATTCCAACCCC	ATCGCTGGAACTCCGAACAG
Lad1	AGAAACACCCTTAACCCGCA	CAGACGCAGATTCTCCTTTCG
Rab15	GATGTGCTGTTCCGGCTACT	GCTCGCCGATAGTACTGCTT
Tnk1	CCCATCACTATCATTGAGGGCA	ATCTTCGTTCTGTGGCTCCG
1600014K23Rik	TGACCCTTGGGAGAATTGCC	GCAGAAGGCTCTGGTTGAGT
Actb	CTAAGGCCAACCGTGAAAAG	TCTCAGCTGTGGTGGTGAAG
Tex19.1	CCATGGGGAACAGACGAAGA	ACATAAAGGGACCCCAATCCC
Grhl2	ACCATCGGGAACATTGAAGA	TCCGGTCCTCTGTAGGTTTG
Tfap2a	CATCGAGGACGTCCCGCACG	TCCCTGGCTAGGTGGACGGC

Table S8. ChIP qPCR primer sequences for validation of the GRHL2 ChIP-seq peak regions. Related to Fig. 5.

Target gene	Forward primer sequence 5' to 3'	Reverse primer sequence 5' to 3'
Spint1	ATCTCCTCAGCCCTGGTTTG	GAGCCAGTTGGACAGGAGTT
Plac1	ATGGTCAGACCCAGGGAAGA	TAGGAAACCGCTGCAGAACC
Prom2	GGCCGTGCATCCTTCTGTAG	GGAGCCCAAACCTGTCGG
Tmem54	CGATGGAGACCCCTTAGAGC	CAGGCCGCCCTCGTTC
Tcfap2a	GCGGGCTTAGAGTTGTCTGA	CTGGTTGTCGGAACAAGCG
Ldoc1	TGCTCTGAAACTCACTTTGGC	AGGGACCTGGAAAATCGCTG
Tex19.1	CAGAGGAACGTTGCTACACCA	ATCAGTGAGCAGCATCGCAG
Kcnk1	CAACATCACCCAGGCCAGT	TGTCTATGGTGGAGGAGGGAT
Tnk1	ACTCTGCTTTCCTCATAGCCC	GTAAGCCAAAATCTGGCCCC
Smpdl3b	TCCTCCAATCAAGCGCACG	AGTTATCCTTGGCGGATGGC
1600014K23Rik	ATCTGTAGCGCACTCCAAAGTT	CCTGGAAAGCCAATCACAGGAA
Lad1-peak1	AGCTCTTGGGTTTCTGCCG	GAACCCAAAGATCGGGGTCA
Lad1-peak2	CAGCCCCACCTAGTGGATAAG	GGGTTGTGACAGGCCAATCT
Rab15	TAGGCTCACCTGGTTCTCCG	CCCCTCCCCACTCTGAAGAA
Control locus	CGTGGCTCATGTGTCAACTAA	CGATGGGACATGGTAGTGTCT

Supplementary Experimental Procedures

Microarray analysis

Total RNA from E7.5 trophectoderm-derived tissues and E9.5 placenta was isolated using the RNeasy Mini Kit (Qiagen, Hilden, Germany) according to manufacturer's instructions including treatment with RNase-free DNase I (Qiagen, Hilden, Germany). Subsequently, RNA was amplified for hybridization with Illumina® MouseWG-6 v2.0 Expression BeadChips (San Diego, CA, USA) using the Ambion® Illumina® TotalPrep™ RNA Amplification Kit (Life Technologies, Darmstadt, Germany). After quantile normalization of the data, we filtered out the genes with a valid RefSeq ID (referring to the annotation file provided by Illumina; http://www.switchtoi.com/annotationfiles.ilmn) and with a *P*-value of the respective log2-transformed expression values less than 0.05 using Student's t test. For heat-map generation, gene expression values were maximum normalized on a per-gene basis for E7.5 and E9.5, separately.

The publicly deposited data samples from human placenta were downloaded from GEO (http://www.ncbi.nlm.nih.gov/geo/), namely the sets under the following URL's: http://www.ncbi.nlm.nih.gov/sites/GDSbrowser?acc=GDS4037, http://www.ncbi.nlm.nih.gov/sites/GDSbrowser?acc=GDS3467 and http://www.ncbi.nlm.nih.gov/sites/GDSbrowser?acc=GDS2990 (Huuskonen et al., 2008; Mikheev et al., 2008; Founds et al., 2009). For our analysis, we only compared probes with the same Affymetrix ID. Log2 transformed data was re-transformed if necessary. As mentioned in the text, the potential GRHL2 target genes show a high correlation with *Grhl2* itself and among each other. The high correlation coefficients of all targets with *Grhl2* are with a probability of less than 0.01 due to random effects. For this *P*-value, correlation coefficients of all genes from the datasets with *Grhl2* have been calculated. Clearly, taking n genes randomly from the dataset and having m ($m \leq n$) correlation coefficients above a level r0 follows a hypergeometric distribution. Setting r0 to be the minimum correlation coefficient among the core target module and having m=n=12 (plus number of genes and number of genes with a correlation coefficient $\geq$r0), led to the respective *P*-value.

Biocomputational analysis of ChIP sequencing

Following initial quality filtering and genome alignment using Bowtie software (Langmead et al., 2009), we obtained around 30 million aligned reads per experiment. To predict GRHL2-associated genomic regions, we used MACS for peak analysis (Zhang et al., 2008) on GRHL2 ChIP samples and on IgG control ChIP samples as background control (threshold *P*-value $1x10^{-5}$). This yielded 5,282 peaks from mouse placenta. The peaks were ranked according to the intrinsic scores provided by MACS (negative log10 transform of the peak's *P*-value). Motif finding was then performed using MEME (Bailey et al., 2009) in the top 10% of all peaks in a 50 bp window around the peak's summit and optimized for de novo detection of 8-9 bp motifs. Motif enrichment in a given sequence set was done by using MAST (Bailey and Gribskov, 1998) and FIMO (Grant et al., 2011). The resulting GRHL2 motif was subjected to TOMTOM analysis (Bailey et al., 2009) for comparison with known transcription factor recognition matrices. Visualization of the ChIP data was carried out using the Integrative Genome Viewer provided by the Broad Institute (Robinson et al., 2011).

For the functional characterization of the GRHL2 ChIP peak at the 3' end of *Spint1*, we used H3K4me1 and H3K27ac ChIP-seq data on mouse placentas from ENCODE. The respective files can be found under wgEncodeLicrHistonePlacH3k04me1FAdult8wksC57bl6StdPk and wgEncodeLicrHistonePlacH3k27acFAdult8wksC57bl6StdPk. We did not use the provided peak tracks and computed them using MACS with the same parameters as for our own data.

Further analysis and visualization of microarray and ChIP-seq data

After peak finding, we found peak-related genes using the closest method of the bedtools suite (Quinlan and Hall, 2010). The respective gene coordinates were obtained from the refGene table of UCSC table browser (http://genome.ucsc.edu/cgi-bin/hgTables?command=start). Setting a distance threshold of 2 kb produced a list of genes near a ChIP peak area. Analysis of our gene expression data also produced gene lists. We then performed an ID conversion using DAVID to entrez gene ID (Huang da et al., 2009b, a) and a manual conversion of gene names not matched by DAVID using the RefSeqGene web page (http://www.ncbi.nlm.nih.gov/refseq/rsg/). After this, the respective lists were intersected to yield the desired target gene set. All list operations were done by self-written Python

programs. The visualization as well was performed by self-written programs in Python using the matplotlib package (http://matplotlib.org/).

ChIP peak annotation to the respective genomic regions (Promoter/TSS, Intergenic etc.) was done using the HOMER software package (Heinz et al., 2010). Random genomic intervals were generated using the shuffle method in the bedtools suite.

Animals

Mice with a conditional (floxed) *Grhl2* allele were obtained from embryonic stem (ES) cells containing a targeted *Grhl2* gene with the fourth exon flanked by loxP sites (see supplementary Material Fig. S5A). Upstream from the floxed exon 4, a neomycin resistance sequence (*neo*^{r}) flanked by two FRT sites was integrated for positive selection. The targeted ES cell clones were generated by electroporation and integration of the targeted construct into the genome of mouse KV1 ES cells (derived from 129B6 hybrid mice) through homologous recombination. Random integration was reduced by the presence of a diphtheria toxin A (*dta*) cassette at the 5' end of the construct. Following G418 selection, a screening for ES cell clones positive for homologous recombination was carried out by PCR using primers depicted in supplementary Material Table S5. A positive ES cell clone was injected into C57BL/6 blastocysts to generate *Grhl2*$^{flox/+}$ mice via standard procedures. Excision of *neo*^{r} was achieved through breeding of *Grhl2*$^{flox/+}$ mice with Flp deleter mice (Farley et al., 2000). *Grhl2*$^{flox/flox}$ mice were viable and fertile. Breeding of female *Grhl2*$^{flox/flox}$ mice with heterozygous *Grhl2*$^{+/-}$ males carrying the *Sox2Cre* transgene (*Sox2Cre;Grhl2*$^{+/-}$) enabled selective *Grhl2* inactivation in the epiblast-derived mouse embryo corpus and in the epiblast-derived extra-embryonic membranes (amnion, yolk sac, allantois) without impairment of the trophectoderm-derived trophoblast lineages through generating *Sox2Cre;Grhl2*$^{\Delta/-}$ mice (Hayashi et al., 2002). *Grhl2*$^{flox/flox}$ and *Sox2Cre;Grhl2*$^{\Delta/-}$ mice were on a mixed 129/C57BL/6 genetic background. Genotyping was done by PCR with primers indicated in supplementary Material Table S4. For timed pregnancies, breeding females were checked for vaginal plugs in the morning. The plug date was considered as embryonic day 0.5 (E0.5).

Antibodies

The following antibodies were used: anti-GRHL2 (HPA004820, Sigma-Aldrich, Hamburg, Germany, 1:200 (immunofluorescence), 6 µg per immunoprecipitation), anti-cleaved caspase 3 (G7481, Promega, Mannheim, Germany, 1:250), anti-CD71 (MCA1033GA, AbD Serotec/MorphoSys AG, Puchheim, Germany, 1:150), anti-MTP1 (MTP11-A, Alpha Diagnostic, San Antonio, Texas, 1:150), anti-pan-cytokeratin-FITC (F3418, Sigma-Aldrich, Hamburg, Germany, 1:100), anti-laminin (L9393, Sigma-Aldrich, Hamburg, Germany, 1:150), anti-Ki-67 (M7249, Dako, Hamburg, Germany, 1:200), anti-PECAM1 (550274, BD Pharmingen, Heidelberg, Germany, 1:100), anti-TCFAP2C (sc-8977 (H-77), Santa Cruz, Heidelberg, Germany, 1:200), anti-collagen IV (AB756, Millipore Corporation, Billerica, MA, 1:150), anti-CDH1 (3195S, New England Biolabs, Frankfurt am Main, Germany, 1:250), anti-SPINT1 (AF1141, R&D Systems Inc, Wiesbaden-Nordenstadt, Germany, 1:50), anti-ITGA6 (MCA699GA, AbD Serotec/MorphoSys AG, Puchheim, Germany, 1:150), rabbit Cldn4 (36-4800, Life Technologies GmbH, Darmstadt, Germany, 1:250), rabbit IgG (011-000-003, Jackson ImmunoResearch, Newmarket, UK, 6 µg per immunoprecipitation).

Immunofluorescence staining and confocal microscopy

Cryo-embedded tissues were cut into 16 µm thick sections and subjected to immunofluorescence staining. After incubation of tissue sections in blocking buffer (PBS/1% BSA/0.05% triton-X-100) for 1 hour, primary antibodies were incubated overnight at 4°C. Primary antibodies were detected with secondary antibodies diluted in blocking buffer and labeled by Cy2, Cy3 or Cy5 (Jackson ImmunoResearch, Newmarket, UK). Nuclei were visualized using TO-PRO®-3 iodide (Life Technologies GmbH, Darmstadt, Germany). Fluorescent microscopy was done on an inverted TCS SP5 tandem confocal microscope (Leica Microsystems GmbH, Wetzlar, Germany). For comparing relative intensity of immunofluorescence staining, the z-plane was adjusted for maximal fluorescence intensity, and image acquisition settings were maintained to be identical for all samples.

GRHL2 immunohistochemistry

For immunohistochemistry, we used the EnVision System-HRP (AEC) kit for the use with rabbit primary antibodies (Dako, Hamburg, Germany) according to manufacturer's instructions. Tissues were fixed in PBS/4% PFA for 1 hour at 4°C, dehydrated, embedded in paraffin and cut into 10 µm thick sections. GRHL2 antigen retrieval was done by incubation for 20 minutes at 100°C in 10 mM citrate buffer pH 6.0.

Hematoxylin and Eosin (H&E) staining

Paraffin-embedded tissue was cut into 5 µm thick sections. Before staining, slides were incubated for 30 minutes to 2 hours at 62°C laying upright in a rack to melt off the paraffin wax. After drying for 30 minutes at room temperature tissue sections were dewaxed by incubating two times in toluol for 5 minutes and rehydrated using a descending ethanol series (100% ethanol: 2 x 2 minutes, 96% ethanol: 2 x 2 minutes, 80% ethanol: 1 x 2 minutes, 70% ethanol: 1 x 2 minutes, ddH_2O: 1 x 2 minutes). Tissue sections were then incubated for 2 to 3 minutes in hemalum solution acid according to Mayer and washed for 30 s in tap water for staining of the nuclei. After short incubation in 1% eosin Y/water solution slides were washed again in tap water and covered with glycerin gelatin and cover slip.

Human tissue samples

We included non-laboured placenta samples from complicated and uncomplicated pregnancies delivered by elective Cesarean section at Oslo University Hospital, Oslo, Norway to analyse expression correlation of *GRHL2* and *SPINT1*. The Regional Committee of Medical Research Ethics in Eastern Norway approved the study and informed written consent was obtained from each participant (ref 529-02162). Placental biopsies from a centrally located normally looking cotyledon (from the center of the cotyledon; omitting the maternal surface and fetal membrane tissues) were obtained following Cesarean sections from 56 preeclamptic women and 28 women with normal normotensive and uncomplicated pregnancies.

In situ hybridization

In situ hybridization on placenta tissue sections was carried out as described previously (Hammes et al., 2001; Schmidt-Ott et al., 2007). Riboprobes were produced from the appropriate plasmids (Table S6). Digoxigenin-labeled cRNA was produced using T7 or T3 polymerase as indicated.

RNA extraction, cDNA synthesis and real-time PCR

Total RNA was isolated using RNeasy Mini Kit (Qiagen, Hilden, Germany) according to manufacturer's instructions including treatment with RNase-free DNase I (Qiagen, Hilden, Germany). First-strand cDNA synthesis was carried out from 500 ng of total RNA from each sample as template with the RevertAid™ First Strand cDNA Synthesis Kit (Fermentas/Fisher Scientific, Schwerte, Germany) according to manufacturer's instructions. Real-time PCR was performed using cDNA as template for expression analyses or DNA for ChIP-seq validation, MESA GREEN qPCR MasterMix Plus for SYBR Assay Rox (Eurogentec, Cologne, Germany) and primers at a final concentration of 200 nM each. For primer sequences used for the validation of Illumina microarray results and for the validation of the GRHL2 ChIP-seq peaks see Table S7 and S8, respectively. Relative levels of mRNA expression were normalized for beta-actin mRNA expression for expression analyses or for total input for ChIP experiments and calculated according to the ddCT method. Statistical significance of differences between two groups was analyzed using two-sided Student's t-test.

Electron microscopy

E9.5 placentas were fixed with 3% glutaraldehyde in 0.1 M sodium cacodylate buffer and 2 mM $CaCl_2$ for 24 hours at 4°C. After washing twice in 0.1 M sodium cacodylate buffer for 30 minutes, placentas were post-fixed in 1% osmium tetroxide (OsO_4) in 0.1 M cacodylate buffer for 2 hours. Afterwards, placentas were washed again twice in 0.1 M sodium cacodylate buffer for 30 minutes, respectively. Samples were dehydrated in a graded ethanol series (70% ethanol: 2 x 20 minutes, 90% ethanol: 2 x 20 minutes, 100% ethanol: 2 x 20 minutes) and propylene oxide (2 x 10 minutes) and embedded in Poly/Bed 812^{R} (Polysciences, Eppelheim, Germany). Polymerization was done at 60°C for 2 to 3 days. Ultrathin sections (70 nm) were contrasted with uranyl acetate and lead citrate and examined with a

Morgagni electron microscope (FEI). Digital images were taken with a Morada CCD camera and the iTEM software (Olympus Soft Imaging Solutions GmbH, Münster, Germany).

Analysis of fluorescence intensity

Fluorescence intensity of immunofluorescence-stained tissue sections was analyzed using the image editing software ImageJ. Immunofluorescence images were first converted into grayscale. Then, BCT cells and overlying chorionic trophoblast cells were separately selected using the freeform selection tool and the level of fluorescence in these regions was analyzed. Mean gray values were determined, mean fluorescence of background readings was subtracted and the relative expression levels were calculated and plotted.

Importantly, for comparing different samples, staining procedures of *Grhl2* control and *Grhl2*$^{-/-}$ placenta sections were performed with identical reagents and in parallel. In addition, image acquisition was also done in parallel using identical image acquisition settings and exposure times.

Supplemental References

Bailey, T. L., Boden, M., Buske, F. A., Frith, M., Grant, C. E., Clementi, L., Ren, J., Li, W. W. and Noble, W. S. (2009). MEME SUITE: tools for motif discovery and searching. *Nucleic Acids Res* **37**, W202-W208.

Bailey, T. L. and Gribskov, M. (1998). Combining evidence using p-values: application to sequence homology searches. *Bioinformatics* **14**, 48-54.

Farley, F. W., Soriano, P., Steffen, L. S. and Dymecki, S. M. (2000). Widespread recombinase expression using FLPeR (flipper) mice. *Genesis* **28**, 106-110.

Founds, S. A., Conley, Y. P., Lyons-Weiler, J. F., Jeyabalan, A., Hogge, W. A. and Conrad, K. P. (2009). Altered global gene expression in first trimester placentas of women destined to develop preeclampsia. *Placenta* **30**, 15-24.

Grant, C. E., Bailey, T. L. and Noble, W. S. (2011). FIMO: scanning for occurrences of a given motif. *Bioinformatics* **27**, 1017-1018.

Hammes, A., Guo, J. K., Lutsch, G., Leheste, J. R., Landrock, D., Ziegler, U., Gubler, M. C. and Schedl, A. (2001). Two splice variants of the Wilms' tumor 1 gene have distinct functions during sex determination and nephron formation. *Cell* **106**, 319-329.

Hayashi, S., Lewis, P., Pevny, L. and McMahon, A. P. (2002). Efficient gene modulation in mouse epiblast using a Sox2Cre transgenic mouse strain. *Mech Dev* **119 Suppl 1**, S97-S101.

Heinz, S., Benner, C., Spann, N., Bertolino, E., Lin, Y. C., Laslo, P., Cheng, J. X., Murre, C., Singh, H. and Glass, C. K. (2010). Simple combinations of lineage-determining transcription factors prime cis-regulatory elements required for macrophage and B cell identities. *Mol Cell* **38**, 576-589.

Huang da, W., Sherman, B. T. and Lempicki, R. A. (2009a). Bioinformatics enrichment tools: paths toward the comprehensive functional analysis of large gene lists. *Nucleic Acids Res* **37**, 1-13.

Huang da, W., Sherman, B. T. and Lempicki, R. A. (2009b). Systematic and integrative analysis of large gene lists using DAVID bioinformatics resources. *Nat Protoc* **4**, 44-57.

Huuskonen, P., Storvik, M., Reinisalo, M., Honkakoski, P., Rysa, J., Hakkola, J. and Pasanen, M. (2008). Microarray analysis of the global alterations in the gene expression in the placentas from cigarette-smoking mothers. *Clin Pharmacol Ther* **83**, 542-550.

Langmead, B., Trapnell, C., Pop, M. and Salzberg, S. L. (2009). Ultrafast and memory-efficient alignment of short DNA sequences to the human genome. *Genome Biol* **10**, R25.

Mikheev, A. M., Nabekura, T., Kaddoumi, A., Bammler, T. K., Govindarajan, R., Hebert, M. F. and Unadkat, J. D. (2008). Profiling gene expression in human placentae of different gestational ages: an OPRU Network and UW SCOR Study. *Reprod Sci* **15**, 866-877.

Quinlan, A. R. and Hall, I. M. (2010). BEDTools: a flexible suite of utilities for comparing genomic features. *Bioinformatics* **26**, 841-842.

Robinson, J. T., Thorvaldsdottir, H., Winckler, W., Guttman, M., Lander, E. S., Getz, G. and Mesirov, J. P. (2011). Integrative genomics viewer. *Nat Biotechnol* **29**, 24-26.

Schmidt-Ott, K. M., Masckauchan, T. N. H., Chen, X., Hirsh, B. J., Sarkar, A., Yang, J., Paragas, N., Wallace, V. A., Dufort, D., Pavlidis, P., Jagla, B., Kitajewski, J. and Barasch, J. (2007). beta-catenin/TCF/Lef controls a differentiation-associated transcriptional program in renal epithelial progenitors. *Development* **134**, 3177-3190.

Uhlen, M., Oksvold, P., Fagerberg, L., Lundberg, E., Jonasson, K., Forsberg, M., Zwahlen, M., Kampf, C., Wester, K., Hober, S., Wernerus, H., Bjorling, L. and Ponten, F. (2010). Towards a knowledge-based Human Protein Atlas. *Nat Biotechnol* **28**, 1248-1250.

Zhang, Y., Liu, T., Meyer, C. A., Eeckhoute, J., Johnson, D. S., Bernstein, B. E., Nusbaum, C., Myers, R. M., Brown, M., Li, W. and Liu, X. S. (2008). Model-based analysis of ChIP-Seq (MACS). *Genome Biol* **9**, R137.